At the crossroads of fertility and metabolism

Pascal Froment, Ingrid Plotton, Cecilia Giulivi, Stéphane Fabre, Rita Khoueiry, Nizar Mourad, Sandrine Horman, Christelle Rame, Charlène Rouillon, Jérémy Grandhaye, et al.

At the crossroads of fertility and metabolism: the importance of AMPK-dependent signaling in female infertility associated with hyperandrogenism

Pascal Froment[1], Ingrid Plotton[2], Cecilia Giulivi[3], Stephane Fabre[4], Rita Khoueiry[5], Nizar I Mourad[6] , Sandrine Horman[7] , Christelle Ramé[1], Charlène Rouillon[1], Jeremy Grandhaye[1], Yves Bigot[1], Claire Chevaleyre[1], Remy le Guevel[8], Patricia Mallegol[9], Ramaroson Andriantsitohaina[9], Fabrice Guerif[10], Jérôme Tamburini[11], Benoit Viollet[11], Marc Foretz[11], Joelle Dupont[1]

Address:

[1] CNRS, IFCE, INRAE, Université de Tours, PRC, F-37380, Nouzilly, France

[2] Molecular Endocrinology and Rare Diseases, University Hospital, Claude Bernard Lyon 1 University, Bron, France

[3] Department of Molecular Biosciences, University of California Davis, School of Veterinary Medicine, Davis, CA and the MIND Institute, University of California Davis Medical Center, Sacramento, CA, U.S.A.

[4] GenPhySE, Université de Toulouse, INRAE, ENVT, 31326, Castanet-Tolosan, France

[5] Epigenetics Group, International Agency for Research on Cancer (IARC), Lyon, France.

[6] Pôle de Chirurgie Expérimentale et Transplantation, Université Catholique de Louvain, Brussels, Belgium

[7] Pole of Cardiovascular Research, Institut de Recherche Expérimentale et Clinique, Université catholique de Louvain, Brussels, 1200, Belgium

[8] Plate-forme ImPACcell, Université de Rennes 1, France

[9] SOPAM, U1063, INSERM, UNIV Angers, Angers, France; Federative Structure of Research Cellular Interactions and Therapeutic Applications, SFR 4208 ICAT, Univ Angers, Angers, France.

[10] CECOS, Hôpital Bretonneau, Tours, France

[11] Université de Paris, Institut Cochin, CNRS UMR8104, INSERM U1016, F-75014, Paris, France.

Running title: *Inactivation of AMPK alpha1 and fertility*

Keywords: fertility, granulosa, AMPK; androgens; PCOS

Correspondence should be addressed to:

Dr. Pascal Froment

UMR PRC, Institut National de la Recherche Agronomique, 37380 Nouzilly, France

E-mail: pascal.froment@inrae.fr

Phone: +33 2 47 42 76 20. Fax: +33 2 47 42 77 78

Abstract

Study question: What biological processes are linked to the signaling of the energy sensor AMP-activated protein kinase (AMPK) in mouse and human granulosa cells (GCs)

Summary answer: The lack of α1AMPK in a transformed human granulosa cell line (KGN) impacted cell cycle, adhesion, lipid metabolism, and steroidogenesis whereas in a transgenic mouse model, a hyperandrogenic response was accompanied by higher 3βHSD and p450scc levels in the ovaries and increases in antral follicles. The α1AMPK gene expression from primary granulosa cells from non-obese women with PCOS (Polycystic ovary syndrome) showed a lower expression than those without it.

What is known already: AMPK is expressed in the ovarian follicle, and its activation by pharmacological medications such as metformin inhibits the production of steroids and androgens. PCOS is responsible for infertility in approximately 5–20% of women of childbearing age. Possible treatments for PCOS include reducing body weight, improving lifestyle, and the administration of a combination of drugs (e.g., clomiphene citrate with metformin) to improve insulin resistance.

Study design, size, duration: AMPK signaling was evaluated by analyzing differential gene expression in KGN cells with and without silencing α1AMPK using CRISPR/Cas9. *In vivo* studies included the use of a α1AMPK knock-out mouse model to evaluate the role of α1AMPK in folliculogenesis and fertility. Expression of α1AMPK was evaluated in primary human granulosa-luteal cells from women with and without PCOS.

Participants/materials, setting, methods: α1AMPK was disrupted in KGN cells and a transgenic mouse model. Cell viability, proliferation, and metabolism were evaluated. Androgen production was evaluated by analyzing protein expression of relevant enzymes of

steroid pathway by Western blots and compound levels obtained from i*n vitro* and *in vivo* models by mass spectrometry. Differential gene expression in human GC was obtained by RNAseq. Analysis of *in vivo* folliculogenesis was performed by histology and immunochemistry, including evaluation of the AMH marker. The α1AMPK gene expression was evaluated by qPCR in primary granulosa cells obtained from non-obese women with (n=8) and without PCOS (n=9).

Main results and the role of chance: Silencing of α1AMPK in KGN increased cell proliferation ($p<0.05$, n=4), promoted the use of fatty acids over glucose, and induced a hyperandrogenic response resulting from the upregulation of two of the enzymes involved in steroid production, namely 3βHSD and p450scc ($p<0.05$, n=3). Female mice deficient in α1AMPK had a 30% decrease in their ovulation rate ($p<0.05$, n=7) and litter size, a hyperandrogenic response ($p<0.05$, n=7) with higher levels of 3βHSD and p450scc levels in the ovaries, and an increase in the population of antral follicles ($p<0.01$, n=10) compared to controls. Primary granulosa cells from non-obese women with PCOS had lower α1AMPK gene expression than the control group ($p<0.05$, n=8-9).

Large scale data: N/A.

Limitations, reasons for caution: The human KGN is a not fully differentiated, transformed cell line. As such, to confirm the role of AMPK in GC and the PCOS phenotype, this model was compared to two others: an α1AMPK transgenic mouse model and primary differentiated granulosa-lutein cells from non-obese women undergoing IVF (with and without PCOS). A clear limitation is the small number of PCOS patients utilized in this study and that the collection of primary GC cells was performed after hormonal stimulation.

Broader implications of the findings: Our results reveal that AMPK is directly involved in steroid production in human granulosa cells. In addition, AMPK signaling was associated with other processes frequently reported as dysfunctional in PCOS models, such as cell adhesion, lipid metabolism, and inflammation. Silencing of α1AMPK in KGN promoted folliculogenesis with increases in AMH. Evaluating the expression of the α1AMPK subunit could be considered as a marker of interest in infertility cases related to hormonal imbalances and metabolic disorders including PCOS.

Study funding/competing interest(s): This study was financially supported by Institut National de la Recherche Agronomique (INRA) and the national program « FERTiNERGY » funded by the French National Research Agency (ANR). The authors report no intellectual or financial conflicts of interest related to this work .

Trial registration number: N/A.

Keywords: fertility, granulosa, AMPK; androgens; PCOS

Introduction

Polycystic ovary syndrome (PCOS) is one of the leading causes of female infertility (5–20% of women of childbearing age (El Hayek *et al.*, 2016; Joham *et al.*, 2015)). It is characterized by hyperandrogenism, infertility, anovulation, and/or ovarian cysts, with a broad phenotypic expression (including hirsutism and acne) (Rotterdam ESHRE/ASRM-Sponsored PCOS Consensus Workshop Group, 2004). Nearly 40–60% of patients with PCOS are either overweight or obese (Ehrmann *et al.*, 2006). As such, intervention therapies for PCOS include reducing the body weight, improving the lifestyle, and administering a combination of drugs (e.g., clomiphene citrate with metformin) to overcome insulin resistance and attenuate PCOS-related endocrine and infertility issues (Fulghesu *et al.*, 2012).

Metformin therapy has been used to realign metabolic and hormonal dysfunctions with some positive outcomes after IVF and IVF/ICSI interventions in women with PCOS (Witchel *et al.*, 2019; Abdalla *et al.*, 2020; Wu *et al.*, 2020). Deciphering the mechanisms of metformin's actions in the ovaries has pointed to a critical kinase activated by metformin called the 5′-AMP-activated protein kinase (AMPK) (Tosca *et al.*, 2005, 2007b; Hardie *et al.*, 2016; Faure *et al.*, 2018). Recently, decreases in AMPK protein levels in the ovaries were reported in DHEA-induced PCOS mouse model (Tao *et al.*, 2017) whereas AMPK activators (AICAR, resveratrol, metformin) improved fertility. Moreover, a close functional link was reported for androgen production and AMPK activity in the ovaries from a transgenic mouse model deficient in LKB1, an AMPK activating kinase gene (Tao *et al.*, 2017). Collectively these studies support the notion of a critical role of AMPK in granulosa cells linked to both metabolism and fertility.

AMPK is a serine/threonine heterotrimeric kinase composed of a catalytic α-subunit and two regulatory subunits, β, and γ. All three subunits of AMPK are highly conserved in

eukaryotic species (Hardie *et al.*, 2003; Ghillebert *et al.*, 2011). This kinase is activated when energy reserves are depleted to produce more energy to maintain ATP homeostasis. Activation of AMPK entails the phosphorylation of the α-subunit at Thr172. All three subunits of AMPK are expressed in the ovaries (Tosca *et al.*, 2005; Dupont *et al.*, 2012; Tartarin *et al.*, 2012) as well as in different follicle cell types (granulosa cells, theca cells, and oocytes) and corpora lutea. The expression and localization of AMPK in the ovary are conserved across species, ranging from invertebrates to vertebrates (Guévélou *et al.*, 2013), and within vertebrates, from mammals to birds (Tosca *et al.*, 2006), cows (Tosca *et al.*, 2007a), pigs (Mayes *et al.*, 2007), rodents (Tosca *et al.*, 2005; Downs *et al.*, 2010) and humans (Pellatt *et al.*, 2011).

In a related but separate role, AMPK may control the crosstalk between energy balance and reproduction, both processes affected in PCOS (Bertoldo *et al.*, 2014). For instance, glucose metabolism dysregulation can trigger defects in ovulation and lower oocyte quality (Downs and Mastropolo, 1994; Pesant and Baillargeon, 2011). Few studies explored the role of AMPK in fertility despite that silencing of oocyte-specific α1AMPK leads to a 30% litter size reduction (Bertoldo *et al.*, 2015). The specific deletion of α1AMPK in murine oocytes altered junctional protein expression and some aspects of mitochondrial physiology (Bertoldo *et al.*, 2015). Pharmacological activation of AMPK inhibited the production of progesterone and oestradiol (Tosca *et al.*, 2005, 2007b), and lower steroidogenesis associated with decreased 3β-hydroxysteroid dehydrogenase (3β-HSD) and p450scc gene and protein expression (Tosca *et al.*, 2005, 2007b, 2010). However interesting these studies are, they included the use of cultured granulosa cells obtained from animal models (rodent and bovine species) and the use of AMPK activators may lack target specificity. As such, no studies have shown a direct role of AMPK signaling in ovarian granulosa steroidogenesis *in vivo*.

149 To bridge this gap in knowledge, this study assessed the role of AMPK steroidogenesis,
150 cell proliferation, and survival in *in vitro* and *in vivo* models by silencing the main catalytic
151 subunit of AMPK, α1AMPK, in human granulosa cells, and by utilizing a transgenic mouse
152 model deficient in α1AMPK.

153

Material and Methods

Animals

Adult animals (10 to 16 week-old mice) wild type (α1AMPK$^{+/+}$) or global α1AMPK knock-out mice (α1AMPK$^{-/-}$) were described in Jorgensen *et al.* (Jørgensen *et al.*, 2004). Briefly, an IRES-βgeo cassette (internal ribosomal entry site-β-galactosidase and neomycin phosphotransferase fusion gene) was inserted to delete a part of the catalytic domain of α1AMPK subunit from amino acids 97–157. Mice were maintained under standard conditions of light (12 h light and 12 h darkness) and temperature with *ad libitum* access to food and water. All animal procedures followed the European legislation for animal experimentation (Directive 86/609/EEC) for animal experiments and with French legislation on animal research. The procedure using α1AMPK-deficient mice was approved by the Directeur Départemental des Services Vétérinaires of the Préfecture de Police de Paris (agreement n° 75-886) and the Paris Descartes University ethics committee (agreement n° CEEA34.BV.157.12). The fertility assessment was performed by crossing three month-old wild-type male mouse with two α1AMPK-deficient female mice at the same age for two weeks in the same cage. When a vaginal plug was detected, the mated female was moved to another cage, and then the litter size was counted at birth.

To recover blood and ovarian tissue, 10 to 16 month-old wild-type female animals were killed by cervical dislocation. Ovaries were fixed in bouin solution for histological studies or directly stored at -80°C for molecular biology analysis. Five days after a vaginal plug, a few females were also euthanized to recover embryos (5-day post-coitum (dpc)).

To assess ovaries' response to gonadotropins, oocytes were retrieved following superovulation induction. Mice were injected i.p. with 5 I.U. of equine chorionic gonadotropin (eCG); 46 h

later, they were injected with 5 I.U. of human chorionic gonadotropin (hCG, Intervet, Boxmeer, Holland). At 12 h later, the oocytes were retrieved and counted.

Human primary granulosa cells

Primary human Granulosa-Lutein cells (GC) were obtained from non-obese women (BMI ≤ 30 kg/m^2) with PCOS and without PCOS undergoing *in vitro* fertilization protocols (IVF). The cells were collected from pre-ovulatory follicles during oocyte retrieval. GC were centrifuged and used for culture , or the pellets were frozen at -80°C to analyze αAMPK expression (Table 2). The ovarian stimulation procedure was described in detail previously (Roche *et al.*, 2016). Ethical approval for this study was obtained from the Research Ethics Board of the CHRU Bretonneau and written informed consent was obtained from all patients. No patients received any monetary compensation for participating in the study, and all patients gave written informed consent before using cells for research purposes. The diagnosis of PCOS was established according to the Rotterdam criteria (oligomenorrhea and/or anovulation, clinical and/or biochemical signs of hyperandrogenism, and polycystic ovaries on ultrasonography scan, as well as the exclusion of other aetiologies that mimic the PCOS phenotype) (Rotterdam ESHRE/ASRM-Sponsored PCOS Consensus Workshop Group, 2004; Teede *et al.*, 2018) by qualified personnel. The non-obese women without PCOS underwent fertility treatments due to male hormonal imbalances or tubal obstruction.

Immortalized granulosa cells

Immortalized human granulosa cells (KGN) were kindly provided by Drs. Masatoshi Nomura and Hajime Nawata, Kyushu University, Japan (Nishi *et al.*, 2001). KGN cells maintain most of the physiological characteristics of primary granulosa cells, including

functional FSH receptors and aromatase expression. KGN cells were cultured in Dulbecco's minimal essential medium (DMEM)/F12 medium (Sigma, St. Louis MO) supplemented with 10% fetal calf serum (FCS) and antibiotics (100 IU/mL penicillin, 100 µg/mL streptomycin (Sigma, l'Isle d'Abeau Chesnes, France) in a 5% CO_2 atmosphere at 37°C. Only early passages (under 30) were used. The cells were cultured at 1 million cells/T75cm² for qPCR or Western blot or 96-well dishes (5,000 cells/well for immunocytochemistry and 10,000 cells/well for other assays). The culture medium was changed every 48 h. Silencing of human α1AMPK in KGN cells was performed after infection with lentiviral particles expressing small guide RNA (sgRNA) guides targeting the *PRKAA1* gene (encoding α1AMPK) (GAATGGTACTCTTTCAGGAT), establishing KO-KGN cells, and a non-targeted guide (GTAGGCGCGCCGCTCTCTAC) creating the control cells, called Scr-KGN cells. The sgRNA guides and lentivirus generation were previously described. (Sujobert *et al.*, 2015)(Grenier *et al.*, 2018). Successfully transfected KGN cells were selected by puromycin. Clones were tested for α1AMPK expression by Western blotting and sequencing amplicons surrounding the target sequence on *PRKAA1* exon 7 (sequencing primers: forward: ATCACCAGGATCCTTTGGCA; reverse: TGCTTTCCTTACACCTTGGTG).

A second mutant KGN cell line was established after infection with lentiviral particles expressing firefly luciferase reporter gene under the control of cAMP-responsive element (Cignal Lenti CRE-Luciferase Reporter, S.A. Biosciences, Qiagen, France) named hereafter KGN-CRE-Luc cells. The cAMP-dependent activity was followed by evaluating the production of cAMP (Promega Luciferase Assay Kit, Promega, Charbonnieres, France) in KGN-CRE-Luc cells after 48 h of treatment with an activator (1 mM dbAMP) or inhibitor of AMPK (Compound C, Sigma, l'Isle d'Abeau Chesnes, France). Values were presented as relative luminescence unit/µg protein and expressed as mean ± SEM.

Immunohistochemistry on fixed cells or tissue

Cell proliferation was evaluated by BrdU staining. Cells were labelled with 10 µM BrdU for 24 h (Sigma, l'Isle d'Abeau Chesnes, France), then fixed in 4% PFA/PBS, and BrdU-positive cells were visualized under indirect immunofluorescence. For labeling polarized mitochondria, living cells were incubated 30 min at 37°C with 200 nM MitoTracker Orange CM-H2TMRos(Invitrogen, Fisher Scientific, Illkirch, France). Afterward, they were fixed, and nuclei were stained with 4′,6-diamidino-2-phenylindole (DAPI).

For all other protocols, fixed cells were incubated with PBS/0.1 M glycine for 15 min at room temperature, permeabilized with 0.1% Triton X-100 (w/v) in PBS for 15 min, and non-specific binding sites were blocked in 2% bovine serum albumin (BSA)/PBS for 15 min. Then, cells were incubated overnight at 4°C with the following primary antibodies against phospho-ERK, Glut4, β-cadherin (Cell Signaling Technologies, Beverly, MA, U.S.A.), BrdU and phalloidin (Sigma, l'Isle d'Abeau Chesnes, France), p53, and AMH (Santa Cruz Biotechnology, CA, U.S.A.). Mouse or rabbit IgG (Sigma-Aldrich, l'Isle d'Abeau Chesnes, France) was used as a negative control. All primary antibodies were diluted at 1:100 in 1% BSA/PBS. After incubating with the primary antibody, cells were incubated for 45 min with goat anti-rabbit IgG Alexa Fluor® 555 or anti-mouse IgG Alexa Fluor® 488 antibodies (Invitrogen, Fisher Scientific, Illkirch, France diluted at 1:500 in 1% BSA/PBS). Cells were counterstained with Hoechst 33342 (Sigma-Aldrich, l'Isle d'Abeau Chesnes, France) and examined using standard immunofluorescence microscopy or a high content screening (H.C.S.) imaging system on the ArrayScan VTI HCS Reader (Thermo Fisher Scientific—Cellomics, Pittsburgh, PA, U.S.A.). Analysis was performed on three independent biological replicates, with a minimum of 3,000 cells per well. Analysis of the surface of cells was quantified using a phase-contrast microscope and image analysis software (ImageJ Fiji software, version 1.52, 2018, NIH, U.S.A.). A minimum of 100 cells in three different experiments (n = 3) were analyzed per genotype.

Immunochemistry was performed on embedded ovaries in paraffin sectioned with a 7-µm slice thickness. Deparaffinized sections were hydrated, microwaved for 5 min in an antigen unmasking solution (Vector Laboratories, Inc., AbCys, Paris, France), and cooled at room temperature. After two washes with PBS for 5 min each, non-specific background was removed by incubation in 2% BSA/PBS for 30 min. Sections were incubated overnight at 4°C with PBS containing primary antibody (1:100) against β-catenin, *N*-cadherin (Cell Signaling Technologies, Beverly, MA, U.S.A.), and AMH (Santa Cruz Biotechnology, CA, U.S.A.). The following day, sections were incubated with a second fluorescent antibody cited above. Measurements from different sections per animal (three animals per genotype) were analyzed using ImageJ Fiji software.

Colony formation assay and migration assay

A total of 10,000 cells were plated in 6-well plates, cultured in 10% FCS, DMEM/F12. Cells were allowed to form colonies up to 1–2 weeks, with media being replaced every 48 h. Colonies were stained with 0.2% crystal violet in methanol, dried, and the colony surface was analyzed with ImageJ Fiji software.

Migration of KGN cells was assessed using a scratch assay. Cells were seeded into 12-well tissue culture dishes at 5×10^5 cells per well. At confluence, a linear scratch was generated by using a sterile tip. Then, cells were incubated with fresh culture medium 10% FCS for 4, 8, and 24 h at 37°C with 5% CO_2. The data were analyzed using ImageJ Fiji software to estimate the migration distance (µm).

Transepithelial electrical resistance (TEER)

KGN cells were cultured at confluence in 24 well tissue culture inserts (0.4 μm pore size, WWR, Fontenay sous Bois, France). TEER was collected with Millicell-ERS apparatus and MERSTX01 electrodes (Millipore, Fisher Scientific, Strasbourg, France). The culture was equilibrated at room temperature before the evaluation. Blanks were considered wells with Hank's buffered salt solution (Invitrogen, Cergy Pontoise, France), and the background was composed of empty wells. TEER was calculated according the following equation: TEER (Ohm/cm^2) = (Rtotal-Rcontrol) x A^{-1}. 'Rtotal' is the resistance recorded, 'Rcontrol' is the resistance of the background, and 'A' is the surface of the insert (i.e., 0.33 cm^2). Four independent biological replicates and technical triplicates were performed in total.

Cell apoptosis and reactive oxygen species assay

Apoptosis was determined by evaluating the activity of the cleaved form of caspase-3, a mediator of programmed cell death, by using the commercial Caspase-Glo™ 3/7 Assay (Promega, Charbonnieres, France). Analysis was performed on six different cultures in duplicate for each condition.

The ROS-Glo™ H_2O_2 Assay (Promega, Charbonnieres, France) was used to evaluate oxidative stress in cells after 48 h of culture by using a luminescent microplate reader (Luminoskan Ascent, V.W.R. International, France).

Metabolites and Steroid Analysis

296 Glucose uptake was evaluated by using the Glucose Uptake-Glo™ Assay (Promega,
297 Charbonnieres, France). Lactate concentrations in the culture medium and pyruvate and
298 cholesterol contents in granulosa cells were evaluated by using the following
299 spectrophotometric assays, respectively (Sigma, l'Isle d'Abeau Chesnes, France; Clinisciences,
300 Nanterre, France; Biolab, Maizy, France). Analysis was performed on at least three different
301 cultures in duplicate for each condition. The results of each assay were normalized per 10^6 cells.

302 Steroid (pregnenolone, 17α-hydroxypregnenolone, dehydroepiandrosterone, 17α-
303 hydroxyprogesterone, Δ4 androstenedione, testosterone, and dihydrotestosterone) levels were
304 determined by LC-MS/MS (mmol/L) as described by Meunier *et al.* (Meunier *et al.*, 2015).

305 The serum AMH level was evaluated on five control and three transgenic mice by using an
306 enzyme-linked immunoassay (AMH Gen II assay®) and read with a Beckman Coulter®
307 (France) as already described in mice (Valeri *et al.*, 2020). The values are expressed in pmol/l.

308

309 **Mitochondrial oxygen consumption (JO_2)**

310 Live, cultured KGN cells were resuspended at a density of 1 x 10^6 cells x mL^{-1}. The JO_2 (pmol
311 O_2 x (s x 10^6 cells)$^{-1}$) was recorded at 37°C with a high-resolution Oxygraph-2K respirometer
312 (Oroboros, Innsbruck, Austria), and data were acquired with DatLab4 software. The cell's basal
313 respiration rate was determined by measuring the linear velocity of oxygen consumption, which
314 reflects the cell's aerobic metabolic activity with physiological substrates in the culture medium.
315 Oligomycin (0.5 µg/mL) was then added to determine the respiration uncoupled to ATP
316 synthesis JO_2 (basal JO_2 minus oligomycin-insensitive $JO_{2)}$. The uncoupled (maximum)
317 respiratory rate was assessed by stepwise additions of carbonyl cyanide *m*-
318 chlorophenylhydrazone (FCCP; 1–2 µM) up to an optimal concentration that represented the
319 capacity of the respiratory chain without the regulation of ATP synthase.

320

321 **Western immunoblotting**

322 Whole ovaries, embryos at 5-dpc, oocytes, and granulosa cells were lysed and exposed to three
323 freeze/thaw cycles in a lysis buffer. After centrifugation, the supernatants' protein concentration
324 was determined using a colorimetric assay (DC assay kit; Uptima Interchim, Montmuçon,
325 France). Equal amounts of proteins were loaded onto 12% SDS-PAGE under reducing
326 conditions then transferred onto nitrocellulose membranes (Schleicher & Schuell, Ecquevilly,
327 France) by following the protocol described before (Tartarin *et al.*, 2012). After that,
328 membranes were incubated overnight at 4°C with the following primary antibodies:
329 phospho-αAMPK (Thr172), proliferating cell nuclear antigen (PCNA), phospho-CREB (Ser
330 133), β-catenin (Cell Signaling Technologies, Beverly, MA, U.S.A.), α1AMPK (Upstate
331 Biotechnology Inc, Lake, Placid, NY, U.S.A.), vinculin (Sigma-Aldrich, l'Isle d'Abeau
332 Chesnes, France), anti-Müllerian hormone (AMH) and 3β-hydroxysteroid dehydrogenase
333 (3βHSD) (Santa Cruz, CA, U.S.A.); steroidogenic acute regulatory protein (StAR) and anti-
334 p450 side-chain cleavage (p450scc) antibodies were generously provided by Dr. Dale
335 Buchanan Hales (Department of Physiology and Biophysics, University of Illinois at Chicago,
336 Chicago, IL, U.S.A.). All commercial antibodies were used at 1:1000 dilution in Western
337 blotting, except 3βHSD antibodies at 1:500 dilution. Signal was detected by enhanced
338 chemiluminescence (Amersham Pharmacia Biotech, Orsay France), and the band densities
339 were quantified using ImageJ Fiji software (N.I.H., U.S.A.). The results are expressed as the
340 intensity signal in arbitrary units after normalization by an internal standard (α1AMPK protein
341 or vinculin) and correspond to the average of three different experiments.

342

343 **High-throughput RNA sequencing**

The 20 RNA sequencing libraries were constructed from 1 µg of total RNA extracted from Scr-KGN cells or KO-KGN cells using Illumina TruSeq RNA Sample Prep (Illumina, San Diego, CA, U.S.A.). Sequencing was performed on an Illumina HiSeq 3000 apparatus using the Illumina TruSeq Standard mRNA kit v2 to obtain stranded paired-end reads (2 x 150 bp). The analysis pipeline of sequence data was performed using the local instance of Galaxy (https://galaxyproject.org) at the Toulouse Midi-Pyrénées bioinformatics platform (http://sigenae-workbench.toulouse.inra.fr/) as already described (Talebi *et al.*, 2018). The FastQ files and metadata were submitted to the European Nucleotide Archive (ENA) at EMBL-EBI under accession number PRJEB46048 (https://www.ebi.ac.uk/ena/browser/view/PRJEB46048).

The cleaned paired-end reads were combined and mapped using STAR2 against the human genome assembly (GRCh38.p13) annotated with the Ensembl *Homo_sapiens* GRCh38.104 annotation version. For each time condition (Scr-KGN cells and KO-KGN cells), the 20 files (n = 10 for Scr-KGN samples and n = 10 for KO-KGN samples) with raw counts were merged to obtain a final count file for statistical analysis of differential gene expression under AMPK depletion.

Differentially Expressed Gene analysis

SARTools R package 1.3.2 (Varet *et al.*, 2016) was used for the descriptive and diagnostic analyses, keeping all samples. Raw counts were pre-filtered for low counts by keeping genes with at least 1 count per million across 10 out of 20 samples, and counts were normalized for library size. A generalized linear model was fitted on the normalized raw count data using the DESeq2 R package version 1.12.3 (Love *et al.*, 2014) to identify the differentially expressed genes (DEGs) between control Scr-KGN (n = 10) and KO-KGN (n = 10) cells. The raw P-

values were adjusted for multiple testing using the Benjamini-Hochberg procedure to control for the false discovery rate (FDR) ("Controlling the False Discovery Rate: A Practical and Powerful Approach to Multiple Testing," 1995). Genes with an adjusted P-value lower than 0.05 (FDR < 5%) were considered as DEGs and selected for subsequent analyses using Metascape (http://metascape.org/). Metascape is a gene annotation and analysis resource (Zhou *et al.*, 2019) to perform functional enrichment analysis, including a canonical, KEGG, and Reactome pathway analysis of the overlapping (DEGs) in all three databases.

RNA extraction, Reverse transcription, and *Real-time quantitative PCR (qPCR)*

Total RNA from granulosa cells was extracted with Trizol reagent (Invitrogen, Cergy Pontoise, France). Total RNA (1 µg) was denatured and retrotranscripted with Moloney murine leukemia virus (MMLV) reverse transcriptase, 15 U (Promega, Charbonnieres, France) in a 20 µl reaction mixture containing 50 mM Tris-HCl (pH 8.3), 75 mM KCl, 3 mM $MgCl_2$, 200 µM dNTP (Amersham, Piscataway, NJ), 50 pmol of oligo(dT)15 and 5 U of ribonuclease inhibitor at 37°C for one h. Targeted cDNAs were quantified by real-time PCR using SYBR Green Supermix (Bio-Rad, Marnes la Coquette, France) and 250 nM of specific primers (Table 1). Each reaction was performed in duplicate and included a negative control (without template DNA). The cycle threshold (Ct) values were calculated automatically and analyzed using CFX Manager™ Software (version 3.1). The relative cDNA number was calculated using the geometric mean of the Ct values from the following normalizing genes ACTB, EEF1A1, and GAPDH (Vandesompele *et al.*, 2002).

Statistical analysis

391 All data are presented as means ± SEM. Unpaired Student's t-test was used to compare the two
392 genotypes (KO-KGN cells vs. Scr-KGN cells or WT mice vs. KO mice). In the case of variance
393 heterogeneity, the Mann and Whitney U test was used to compare means between two groups.
394 Values were determined to be significant when $p \leq 0.05$; *, $p < 0.05$; **: $p < 0.01$; ***:
395 $p < 0.001$.

396

397

Results

1. Confirmation of the silencing of α1AMPK in human granulosa cells

To assess the role of AMPK on granulosa cells, we silenced the main catalytic subunit of AMPK α1AMPK in human KGN cells by using the sgRNA system developed by Tamburini(Grenier *et al.*, 2018). Sequencing the *PRKAA1* gene confirmed the presence of a sgRNA-induced mutation in exon 7 (**Figure 1A**). The KO-KGN clone showed negligible α1AMPK Thr172 phosphorylation and α1AMPK protein levels (**Figure 1B**).

2. *In vitro* silencing α1AMPK stimulates proliferation, adhesion, and faster migration in KGN cells

We first investigated the effects of silencing α1AMPK on cell viability and proliferation. While KO-KGN cells did not undergo apoptosis or stabilize tumor protein 53 (*TP53*; **Supplemental Data 1A and 1B**), they showed higher proliferation evidenced by the greater cell colony area (1.4-fold higher; $p < 0.01$, **Figure 2A**); higher number of $BrdU^{-}$positive cells (2-fold; $p < 0.05$) (**Figure 2B**); higher percentage of cells with phosphorylated-ERK (**Figure 2C**); and higher content of PCNA ($p < 0.05$) (**Figure 2D**). The hyperproliferation was associated with a reduction of the size of granulosa cells (**Figure 2E**) and a migration estimated (by the scrap assay) 16% faster at 24 h than that in Scr-KGN cells ($p < 0.05$) (**Figure 2F**). Additionally, the cell-cell adhesion of KO-KGN cells was more robust than that of Scr-KGN cells supported by the increased electrical resistance of the cell layer evaluated by TEER (**Figure 2G**) and the higher β-catenin content observed by immunochemistry and Western blot (**Supplemental Data 1C and 1D**).

3. Silencing **α1AMPK alters glucose metabolism in KGN**

It has been reported that hyperproliferation is associated with lower mitochondrial energy metabolism such as described for cancer cells *(Faubert* et al*., 2015)*. In support of this concept, hyperproliferative KO-KGN cells had a modest lower polarized mitochondria density per cell (13% decrease, $p < 0.05$) than Scr-KGN cells (**Figure 3A**) suggesting that silencing AMPK did influence mitochondrial mass significantly. However, the ATP-linked oxygen consumption rate under basal conditions in KO-KGN cells was half than that of Scr-KGN cells, and the uncoupled or maximal rate in KO-KGN cells was 0.7-fold of that of Scr-KGN cells ($p < 0.05$; **Figure 3B**). The lower electron transport capacity (phosphorylating and non-phosphorylating) was associated with a 40% reduction in the levels of hydrogen peroxide (H_2O_2) and reactive oxygen species (ROS. ($p < 0.01$), as well as a 20% reduction in Cellrox immunostaining, a fluorescence probe activated by ROS ($p < 0.05$) (**Supplemental Data 2**). These results indicated that silencing AMPK signaling had a more profound impact on mitochondrial function (30 to 50%) than on mitochondrial mass (13%).

In addition, lower glucose uptake was observed in KO-KGN cells (by 70%; $p < 0.05$) associated with a reduction in the expression of the glucose transporter insulin-dependent GLUT4 (by 30%; $p < 0.01$) (**Figure 3C and 3D**). Despite the lower glucose uptake, activation of glycolysis is inferred by the substantial increase in lactate in KO-KGN cells compared to controls (1.8-fold). The higher pyruvate levels in KO-KGN cells compared to Scr-KGN cells is suggestive of lower activity of the pyruvate dehydrogenase complex (**Figures 3E and 3F**), probably as a result of higher PDH kinase activity and/or lower mitochondrial function. Indeed, *in vivo* studies suggested that AMPK regulates pyruvate entry into the mitochondrion (Klein *et al.,* 2007; Buresova *et al.,* 2020).

4. Silencing AMPK stimulates steroidogenesis in KGN cells

The primary function of granulosa cells is the production of steroids, which evolve during follicular maturation. The cholesterol content, precursor molecule of steroid synthesis, was 30% higher in KO-KGN cells (**Figure 4A**). This higher cholesterol content seemed to facilitate androgen production (6-fold) supported by the higher levels of Delta4 androstenedione (D4), testosterone (TS), and dihydrotestosterone (DHT) ($p < 0.01$) (**Figure 4B**). This hyperandrogenism was associated with higher expression of two enzymes involved in steroid production (p450scc and 3βHSD), 1.2- and 1.7-fold, respectively, in KO-KGN cells compared to Scr-KGN cells ($p < 0.05$) (**Figure 4C and 4D**), without changes in the expression of the cholesterol carrier StAR. Taken together these results show that silencing AMPK increases steroid enzymes' contents. This is also supported by the 3-fold increase in a cAMP-dependent factor, the pSer-133 CREB transcription factor ($p < 0.01$) (**Figure 4C and 4D**), and the induction of the reporter gene (luciferase) driven by the cAMP response element (the response element for CREB**)** under both basal and dbAMP-stimulated conditions ($p < 0.05$) (**Figure 4E**) when AMPK was inhibited by Compound C.

5. Silencing AMPK alters the transcriptome of KGN cells

In order to get a global view of the consequences of the absence of AMPK, we performed RNA sequencing. RNAseq analysis has revealed 1237 DEG (differentially expressed genes) (541 DEG down regulated in KO group , 696 DEG up regulated in KO group) with a $P<0.05$. Genes are involved in the cytoskeleton, extracellular matrix, cell cycle, cell proliferation, cell locomotion, monocarboxylic acid metabolism, lipid metabolism, steroidogenesis, and inflammatory response (**Figure 5A ;** volcano-plot, **s**ee **Supplemental Data 3)**. The results were confirmed and validated by following the gene expression of six

candidate genes (interleukin-6, superoxide dismutase 2, Pentraxin 3, collagen type IV alpha 6 chain, matrix metallopeptidase 11, and creatine kinase; **Supplemental Data 4**). Biological processes enriched in the KO-KGN cells showed the interaction between cytoskeleton reorganization, metabolism, lipid processes, and immunity processes (**Figure 5B)**. Relevant genes associated with lipid and steroid production were ELOVL7, HSD11B1, CPT1A, and perilipin 2, including androgen-induced genes, such as vanin 1, genes related to the extracellular matrix (COL4A5 and COL4A6) and pro-inflammatory genes (IL-6, IL-1B, CCL20, and CXCL1). Interestingly, a total of 42 down-regulated genes and 14 up-regulated genes in KO-KGN cells have already been reported in a PCOS database developed from the literature (PCOSbase) (**Supplemental Data 5**). Gene expression have been confirmed in human primary granulosa-lutein cells exposed to AMPK inhibitor and also rescued after AMPK re-expression (**Supplemental Data 6-8**).

6. Fertility of α1AMPK$^{-/-}$ female mice is reduced

To place the effects of AMPK in a physiological context, we investigated the fertility of female α1AMPK-deficient mice (**Figure 6A**). The number of live pups per litter was decreased by 30% in α1AMPK$^{-/-}$ female mice in comparison to controls ($p < 0.05$) (**Figure 6B**), and associated with a similar decrease in the number of corpora lutea (**Figure 6C**). To evaluate the ovary's response independently of the hormones of the hypothalamic-pituitary system, oocytes were collected and counted after superovulation. The oocyte number was lower in α1AMPK$^{-/-}$ mice (21.4 ± 2.4 oocytes) than in control mice (34.2 ± 1.7 oocytes; $p < 0.05$) (**Figure 6D**). Histology of ovaries in α1AMPK$^{-/-}$ mice has shown presence of all type of follicles but more secondary follicles formed a ring around the ovary (**Figure 6E**). Analysis of estrous cycle in transgenc mice revealed a delayed between 2 cycles without change in estrous length (**Figure 6F-G**)

The drop in the ovulation rate allowed us to further evaluate folliculogenesis. Analysis of primary and secondary antral follicles in α1AMPK$^{-/-}$ female mice was increased by 1.3- and 1.5-fold, respectively ($p < 0.01$) (**Figure 7A**). Analysis of atretic follicles by visualization of pycnotic bodies in follicles revealed only an increase in antral follicles (200-300μm), but not in primary follicles (50-199μm) or pre-ovulatory follicles (**Figure 7A and Supplemental Data 9**). This result was confirmed by a high proportion of AMH-positive follicles, a marker of large preantral and small antral follicles, in α1AMPK-/- ovarian tissue ($p = 0.05$) (**Figure 7B and 7C**), and elevated AMH levels in the blood; however, the number of pre-ovulatory follicles was limited in α1AMPK$^{-/-}$ mice (**Figure 7A**). Expression of β-catenin, which is involved in tissue architecture, was decreased in secondary antral follicles from α1AMPK$^{-/-}$ female mice. This was evidenced by changes in the shape and structure of granulosa cells layers, which were not cuboidal as in control mice and had a non-linear distribution (**Figure 7D**).

Consistent with our results with KO-KGN cells, higher levels of steroids and androgens were observed in α1AMPK$^{-/-}$ ovarian tissue and blood compared to those in controls, including testosterone, pregnenolone, 17α-hydroxyprogesterone, and Δ4-androstenedione (**Figure 8A-F**). The expression of enzymes involved in steroid production (p450scc and 3βHSD) was also higher in α1AMPK$^{-/-}$ ovarian tissue (**Figure 9A-C**). These results confirmed the validity of using the KGN based on the overlap of outcomes observed with the α1AMPK$^{-/-}$ mice.

7. α1AMPK content is lower in primary human granulosa cells from non-obese women with PCOS

To compare the results obtained *in vitro* with those *in vivo*, we evaluated the gene expression of α1AMPK and α2AMPK in primary human granulosa cells retrieved from non-obese women with and without PCOS, both obtained through IVF protocols. As shown in **Figure 10A,** a significant 63% reduction in α1AMPK mRNA expression was observed in

PCOS granulosa cells in comparison to control cells ($p < 0.05$), with no statistical differences in the gene expression of α2AMPK. The α1AMPK protein content was slightly but significantly lower in PCOS granulosa cells (by ~25%) (**Figure 10B**).

Discussion

Our work illustrates the importance of α1AMPK for granulosa cell functions and the potential link with the development of the PCOS phenotype. *In vitro* inactivation of α1AMPK in human granulosa cells leads to changes in the gene expression of proteins involved with the cytoskeleton, extracellular matrix, cell cycle, immune system, monocarboxylic acids, and lipid metabolism. This differential expression may explain the issues observed with cell maturation, glucose metabolism, inflammation and steroid production (**Figure 11**). This phenotype obtained with a disrupted AMPK axis overlaps with those described in women with PCOS (e.g., formation of cysts in the ovary, hyperandrogenism, and insulin resistance (Sirmans and Pate, 2013)).

To decipher more precisely the role of AMPK in granulosa cells function, we chose to limit the use of pharmacological interventions which despite their inhibitory effect on AMPK may have unintended effects on other kinases. Instead, we developed a strategy to mutate α1AMPK gene in human granulosa cells that conserved some properties as the primary cells such as FSH-sensitivity, steroid production, and expression of AMH. These cells have the disadvantage of being transformed linked to other gene mutations. Primary granulosa cells from transgenic mice or human granulosa-lutein cells might also have been available for our study but they present some disadvantages as well. Human granulosa-lutein cells are retrieved after hormonal treatment and are differentiated cells with high steroids production and low proliferation rates; the mouse primary granulosa cells proliferate slowly; and cells preparation consistency across mice is an issue as well as obtaining follicles at the same stage of differentiation at the moment of retrieval. The advantage of primary cells used here overcomes the disadvantage of using heterogenous cell populations associated with lower efficiency in

gene manipulation resulting in a mosaic population which may mask the actual effect of the silencing. We confirmed the results obtained with KGN by using a pharmacological inhibitor drug (compound C or SBI-0206965) on primary GC in culture (**supplemental data 6-8**) and *in vivo* with ovaries from transgenic α1AMPK$^{-/-}$ mice, confirming the disruption of steroid production and adhesion or migration of granulosa cells.

Transcriptomics and biological approaches on KGN cells showed the impact on three main functions: the extracellular matrix and cell proliferation, energy metabolism which has repercussions on steroid production, and immune function. This last aspect, not explored here, is worthy of more studies in the future. RNAseq analysis showed dysregulation of genes related to cytoskeleton reorganization (collagen type IV, matrix metallopeptidase 11, CD9 molecule, laminin A/C, destrin, an actin-depolymerizing factor). Laminins and collagen proteins are the most abundant extracellular matrix components of the basal lamina and granulosa cell layers of ovarian follicles (Rodgers *et al.*, 2001). Modifying the cytoskeleton in ovine granulosa cells using pharmacological drugs, induced cell rounding, inhibition of proliferation and progesterone secretion. These observations may support the hypothesis that the cytoskeleton and extracellular matrix play an essential role in granulosa cell luteinization (Le Bellego *et al.*, 2005). Supporting this notion, several studies have shown that the rigidity of the extracellular matrix has negative consequences on follicular activation and its growth (West *et al.*, 2007) and the capacity of migration and adhesion of the cells are critical for the formation of the corpus luteum ((Rolaki *et al.*, 2007) (Franz *et al.*, 2013). In a mouse model of PCOS, granulosa cells have been noted to be arranged loosely in fewer (only 1–3) layers (Tao *et al.*, 2017), as we have observed in our transgenic mouse model. In cultured bovine granulosa cells, among 30 differentially regulated genes related to cell-cell communication were identified by the IPA tool, with genes affected by AMPK signaling when density changes occurred (Baufeld *et al.*, 2017). Also, in our condition, it is possible that the absence of α1AMPK changed the

extracellular matrix and induced signals to stimulate granulosa cell proliferation by stimulating follicular activation as attested by the higher population of pre-antral follicles in α1AMPK$^{-/-}$ mice. Furthermore, a study using an AMPK inhibitor described that incubation of primordial follicles *in vitro* with Compound C increased the growth of the follicle (Jiang *et al.*, 2016). We can compare these data to a recent study in an ovine model that reported a disruption in the extracellular matrix structure in the ovaries induced by a maternal environment rich in androgens and culminated in the acceleration of follicular growth (Monniaux *et al.*, 2020). Similarly, in our α1AMPK$^{-/-}$ mice, a high number of large preantral and small antral follicles were observed with a higher population of AMH-positive follicles in the ovaries. AMH is a well-established specific marker of this subpopulation of follicles, which is also elevated in women with PCOS (Visser *et al.*, 2006; Torres-Rovira *et al.*, 2014) and in PCOS-induced mouse models. Consistent with this view, polycystic ovaries present some abnormalities in the dynamics of follicles and contain higher numbers of primary and secondary follicles (Franks *et al.*, 2008). AMH levels and ovary follicular development could be improved by administering an AMPK agonist, metformin, associated with resveratrol or pioglitazone treatments (Stracquadanio *et al.*, 2018).

As expected, energy metabolism was affected in α1AMPK$^{-/-}$ models (mice and of KO-KGN cells). We reported, in KO-KGN cells, a decrease in glucose uptake, and a lower content of the insulin-regulated glucose transporter GLUT4; and lower mitochondrial metabolism associated with elevated lactate and pyruvate levels. It is now widely recognized that insulin resistance is present in obese or overweight women and often in lean women with PCOS. The data obtained from KO-KGN cells are consistent with other studies showing that the levels of GLUT1 and GLUT3 are lower in PCOS patient-derived iPSCs (Min *et al.*, 2018), and a lower mitochondria content in blood cells of patients with PCOS, which is inversely correlated to the level of insulin resistance (Lee *et al.*, 2011). It is known that metabolic disorders are clinically

596 associated with declining fertility (Estienne *et al.*, 2019). In the present study, we showed a
597 change in the expression of glucose and lipid metabolism enzymes, such as pyruvate
598 dehydrogenase kinase 4 (entry of pyruvate to Krebs'c cyle) and transaldolase 1 (pentose
599 phosphate shunt) by the RNAseq analysis of α1AMPK-deficient human granulosa cells. PDK4
600 is known to be induced by AMPK (Houten *et al.*, 2009) and by phosphorylating PDK, inhibits
601 its activity explaining the higher lactate and pyruvate concentrations in KO KGN cells.
602 Transaldolase 1 is a key enzyme of the pentose phosphate pathway that generates NADPH for
603 DNA and RNA syntheses related to proliferation and growth. Others genes of metabolism such
604 as vanin 1(VNN1), which are regulated by androgens, should be indirectly modified by
605 hyperandrogenism.

606 Interestingly, the most up-regulated gene was ELOVL fatty acid elongase 7 (ELOVL7)
607 gene, which catalyzes the formation of neutral lipids and cholesterol esters as a source of *de*
608 *novo* steroid synthesis. ELOVL7 is also regulated by the androgen pathway through SREBP1
609 (Tamura *et al.*, 2009). We have confirmed the high cholesterol content in granulosa cells and
610 the overall consequence on steroid production both *in vitro* and *in vivo* in α1AMPK$^{-/-}$ transgenic
611 mice. We also noticed a direct consequence on the hyperactivation of the transcription factor
612 CREB and enzyme involved in steroid production. Several studies using pharmacological
613 approaches on granulosa cells described an inhibition of the production of progesterone and
614 oestradiol in rodent and bovine granulosa cells by the two AMPK activators: AICAR or
615 metformin (Bowdridge *et al.*, 2015). Metformin is also used as a treatment for patients with
616 PCOS, restoring ovulation by inhibiting androgen synthesis (Palomba *et al.*, 2005). This
617 inhibition was partly explained by a decrease in the expression of key enzymes, such as 3βHSD,
618 p450scc, and StAR (Tosca *et al.*, 2005), leading to a reduction of androgen synthesis by thecal
619 cells (Attia *et al.*, 2001; Mansfield *et al.*, 2003). Quite recently, the secretion of progesterone

by human mural granulosa cells was shown to be resistant to AMPK inhibition (Bowdridge *et al.*, 2017) .

To investigate the "*in vivo*" possibility of a potential genotype-phenotype correlation, we examined the fertility of transgenic α1AMPK-deficient mice because the phenotype present several PCOS traits, and we have determined the expression of the α1AMPK gene in purified granulosa cells from patients carrying the PCOS phenotype. Indeed, the α1AMPK$^{-/-}$ transgenic mouse model showed irregular cycles, ovulatory dysfunction, dysregulation in folliculogenesis associated to elevated AMH level and excess in androgen production by the ovaries. Interestingly, this phenotype is quite similar to those described in rodent model of PCOS induced by DHEA, where the authors still observed phospho-αAMPK, but a lower total αAMPK concentrations in the ovaries in comparison to control mice (Tao *et al.*, 2017). Another recent work found a reduction in AMPK immunoreactivity in follicles from a group of DHEA-induced PCOS rats compared to a control group (Furat Rencber *et al.*, 2018). The expression of αAMPK could be up-regulated by treatment with metformin and resveratrol and was associated with an improvement of the PCOS phenotype in rat (Furat Rencber *et al.*, 2018). These results suggest that a lower expression of α1AMPK could participate or be associated to the etiology of PCOS. However, despite the human PCOS syndrome is associated to multifactorial factors, several PCOS rodent models have been developed through different strategies and tended to mimic PCOS traits: (i) hyperandrogenism, induced by androgens (DHEA, DHT) injection or using an aromatase inhibitor, which is one of the most important features to induce a PCOS phenotype (Caldwell *et al.*, 2014; Abbott *et al.*, 2019; Rodriguez Paris *et al.*, 2021). More recently, high AMH levels during embryonic stage have shown to induce a PCOS phenotype during adulthood. Indeed, elevated AMH resulted in maternal neuroendocrine-driven testosterone excess and masculinized the female fetus (Tata *et al.*, 2018) ; (ii) by changing diet or stressful environmental conditions ; and (iii) by gene mutation as in

transgenic animal models over-expressing LH or nerve growth factor, or presenting a deletion of PTEN or the plasminogen activator inhibitor-1 (PAI-1) in follicle (Ryu *et al.*, 2019).

In our model, we can hypothesize that deficiency in α1AMPK in female mice increases androgen levels through a higher expression of enzymes involved in steroid production as observed in DHEA or DHT-induced PCOS mouse models and higher AMH levels during pregnancy. These data provide further evidence for the interest to use AMPK activators (adiponectin agonist/inducer, metformin…) in a PCOS treatment or to develop a personalized medicine according to the activity of AMPK in granulosa cells in order to determine the sensitivity of the patient to the treatment and to adapt it. Furthermore, this model is also of interest to study the AMPK pathway and the use of AMPK activators in the etiology of granulosa cancer or development of therapy. It will be interesting to use a strategy to overexpressed AMPK in ovarian follicle of a PCOS mouse model, we can evaluate the importance of the AMPK signalling in the treatment of PCOS trait. Moreover, to perform an inducible deletion of α1AMPK specifically in granulosa cells could help us to decipher the consequence on folliculogenesis if AMPK is absent at early stage (embryo stage) or during adulthood.

In summary, granulosa cells from patients with PCOS have lower gene expression of α1AMPK. Similarly, a disruption of the α1AMPK gene in both *in vitro* human granulosa cells and *in vivo* in transgenic mice results in a PCOS-like phenotype with irregular cycles, changes in follicular dynamics, and hyperandrogenism. These changes in folliculogenesis triggers a reduction in ovulation rate as observed in patients with PCOS or in PCOS-induced mice (Tao *et al.*, 2017). Our study suggests the involvement of AMPK in granulosa cell functions, and a dysregulation of AMPK could be implied in the aetiology of the PCOS phenotype. Therefore,

669 novel insights into the mechanism of PCOS associated with AMPK have to be identified. The
670 development of specific therapeutic targets of AMPK could be of interest to improve the
671 subfertility associated with a metabolic syndrome such as PCOS.

673

674 **Acknowledgements**

675 We thank Dr Dale Buchanan Hales (Department of. Physiology and Biophysics, University of
676 Illinois at Chicago, Chicago, IL, U.S.A.) for generously providing the anti-StAR and anti-
677 p450scc antibodies. We are grateful to Agnes Wiedermann, Fabrice Laurent (INRAE, ISP,
678 Centre Val de Loire) for TEER tool. We would like to thank Julien De Poortere, Emma de
679 Cartier d'Yves and Luc Bertrand for their help with the new mouse experiments. This work
680 was financially supported by Institut National de la Recherche Agronomique (INRA) and the
681 national program « FERTiNERGY » funded by the French National Research Agency (ANR).

682

683

684

685

686 **Figure legends**

687

688 **Table 1. Primers for quantitative Real-Time PCR**

689 **Table 2. Biological parameters of patients from control and PCOS groups.**

690 **Figure 1**. **Mutation of the α1AMPK** (**A**) Sequence of part of exon 7 of the PRKAA1 gene
691 from KGN genomic DNA (location : 40,765,238 to 40,764,752). (**B**) Western blot analysis of
692 phospho-AMPK-alpha (Thr172) and α1AMPK in KO-KGN (mutant cells) and Scr-KGN
693 granulosa cells (control cells). Vinculin was used as control. Results are representative of 3
694 independent experiments.

695

696 **Figure 2**. **In vitro proliferation ability of KO-KGN cells (A)** Comparison of the KO-KGN
697 and Scr-KGN granulosa cells colony formation, cells were plated at a very low density (1.5 ×
698 10^3 cells/well) and 2 weeks later, the surface occupied by foci were quantified (n = 4
699 independent experiments). Representative fields are presented below. **(B)** KGN were cultured
700 in presence of 10 µM BrdU for 24h. The percentage of BrdU positive cells was analyzed by
701 High Content Screening. Results are representative of 6 independent experiments in triplicate
702 with at least 3000 cells counted per well. **(C)** Percentage of phosphorylated ERK positive cells
703 analyzed by High Content Screening (n=3 independent experiments). **(D)** Western blot analysis
704 of PCNA in KO-KGN and Scr-KGN granulosa cells. Vinculin was used as control. Results are
705 representative of 3 independent experiments. **(E)** Representative microscopic fields of KO-
706 KGN and Scr-KGN cell surface. Scale bar = 50 µm. (right panel), Quantification of cell surface
707 (µm²) by ImageJ software (measured on at least 300 cells from 3 independent cultures). **(F)**
708 migration assays. KGN cells were scraped from the culture dish and the mean migration
709 distance of cells was assessed for 24 h. Quantification of the migration distance for KGN cells

is shown as (μm) (n=4). **(G)** KGN cells were cultured at confluence in 24-well tissue culture inserts (0.4 μm pore size) The Trans-epithelial electrical resistance (TEER) was analysed and reported as (Ohm/cm^2) 4 different cultures were performed Values are the mean ± SEM *P <0.05, **P< 0.01, ***P<0.001.

Figure 3.**Mitochondria activity in KO-KGN cells**. **(A)** The mitochondrial membrane potential in KGN cells was analyzed by mitotracker dye. The density and intensity of mitotracker in each cell was quantified by High Content Screening. Results are representative of 3 independent experiments. **(B)** KGN suspension (1×10^6 cells/ml) was transferred into a stirrer 2-ml oxygraph vessel where JO_2 was recorded before and after the successive addition of 0.5 μg/ml oligomycin and 1–2 μm carbonyl cyanide *m*-chlorophenylhydrazone. Data are represented as means ± sem of n = 4 different KGN isolations **(C)** Glucose uptake in KGN granulosa cells was quantified using the Glucose Uptake-Glo Assay after medium change, insulin (100ng/ml) and 30 min incubation with 2DG (2-DeoxyGlucose). (n = 4 independent experiments*)*. **(D)** intensity of Glut4 immunostaining in each cell was quantified by High Content Screening. Results are representative of 3 independent experiments. **(E)** Pyruvate intracellular concentration (ng) per μg protein content (n=3) **(F)** Lactate secretion measured in culture medium conditioned by KO-KGN and Scr-KGN granulosa cells for 48 h (percentage of control normalized per 200,000 cells/well) (n=7). Values are the mean ± SEM *P <0.05, **P< 0.01, ***P<0.001.

Figure 4. **Molecular alteration in steroidogenesis in KO-KGN cells**. **(A)** Intracellular concentrations of cholesterol in KO-KGN and Scr-KGN granulosa cells (n=3). **(B)** KGN granulosa cells were incubated for 48h with dehydroepiandrosterone (DHEA) and the following

steroids were quantified by mass spectrometry: Δ4 androstenedione (D4), testosterone (TS), dihydrotestosterone (DHT) (n=3). **(C)** Western blot analysis and **(D)** quantification of phospho-CREB, CREB, 3β-HSD, StAR and P450scc expression in KO-KGN and Scr-KGN granulosa cells, normalized to vinculin (n=3-5). **(E)** Wild-type KGN cells expressing luciferase under the control of cAMP response element (Cignal Lenti Reporters, Qiagen) (KGN-CRE-Luc) were stimulated for 48h with dbAMP 1mM and / or with the AMPK inhibitor (10µM Compound C). Luciferase assay was performed, and promoter activity values are expressed as relative luminescence units perµg of proteins content. (n=3). Values are the mean ± S.E.M. *P <0.05, **P< 0.01, ***P<0.001.

Figure 5. Gene enrichment analysis in KO-KGN cells.

Biological function processes or networks of related pathways enriched were constructed using the Metascape software **(A)** Heatmap of the top15 of GO enriched terms colored by *P*-values. **(B)** Network of biological processes or related pathways enriched in the KO-KGN cells samples (n=5) which were closely correlated.

Figure 6. **Fertility of α1AMPK-/- female mice**. **(A)** Western blot analysis of the α1AMPK subunit in whole ovary from total knock-out animals (KO, α1AMPK-/-) versus wild-type mice (WT, α1AMPK+/+) (n = 4) **(B)** Fertility analysis of α1AMPK+/+ and α1AMPK-/- females mated with wild-type males (n = 29(KO), n=43 (WT)). **(C)** Number of corpora lutea per female from both genotypes (n = 7). **(D)** Number of oocytes recovered following superovulation treatment in α1AMPK+/+ and α1AMPK-/- females (n = 7 per genotype). **(E)** Histology of ovaries of nontransgenic (left) and homozygotes α1AMPK transgenic mice (right). Bar. 200 µm. **(F)** Estrous cycle pattern in a representative females. P. proestrus; E. estrus; M. metestrus

; D. diestrus **(G)** Average length of estrus cycle and estrus length. Analysis of the AMH serum level. Values are the mean ± SEM *P <005, ***P<0.001.

Figure 7. **Decrease in pre-ovulatory follicles population in α1AMPK-/-**. **(A)** Representative picture of atretic and healthy follicle. Bar 100 µm. And quantification of healthy and atretic follicles in the following range of follicles : primary follicles (50-199µm). antral follicles (200µm-300µm) and pre-ovulatory follicles (≥ 300µm) per ovary were counted in α1AMPK+/+ and α1AMPK-/- ovary (n=10 mice per genotype). **(B)** Immunostaining and quantification of AMH in $\alpha1AMPK^{+/+}$ and $\alpha1AMPK^{-/-}$ ovary (n=5 mice per genotype). **(C)** AMH protein content in whole ovary lysates from $\alpha1AMPK^{+/+}$ and $\alpha1AMPK^{-/-}$, normalized to vinculin. Quantification was shown in the side of the western-blot. (n=4 mice per genotype). **(D)** AMH serum level in α1AMPK transgenic mice **(E)** Immunostaining and quantification of β catenin and N-cadherin in preantral follicles. Quantification of intensity was performed by ImageJ software (n=5 mice per genotype). Values are the mean ± SEM *P <0.05, **P<0.01, ***P<0.001.

Figure 8. **Steroid analysis in α1AMPK-/- female mice**. The following steroids were analysed in blood and whole ovary extract from α1AMPK+/+ and α1AMPK-/- adult females, **(A)** Pregnenolone, **(B)** 17α-Hydroxypregnenolone, **(C)** Dehydroepiandrosterone, **(D)** 17α-Hydroxyprogesterone, **(E)** Δ4 androstenedione , **(F)** testosterone. (n = 7 mice per genotype). Values are in mmol/L or µmol/ovary extract as a mean ± S.E.M. *P <0.05, **P<0.01.

Figure 9. **expression of steroidogenic enzymes in α1AMPK-/- female mice**. **(A)** the cholesterol transporter, StAR, **(B)** p450scc, and **(C)** 3βHSD expression in whole ovary lysates

from α1AMPK$^{+/+}$ and α1AMPK$^{-/-}$, normalized to vinculin. Quantification of the expression of StAR, p450scc, and 3βHSD in both genotypes were shown in the side of the western-blot. (n = 3 mice per genotype) *, $P < 0.05$. Values are the mean ± SEM *P <0.05, **P<0.01.

Figure 10. **Expression of AMPK in primary human granulosa cells**. **(A)** left panel. Testosterone serum level in the obese and non-obese patients (BMI ≤30) and (B.M.I. ≤30). Right panel. mRNA expression of α1AMPK and α2AMPK by RT-qPCR in human granulosa cells retrieved from a group of control non-obese patients (BMI ≤30) (n=8 patients) and a group of PCOS non-obese patients (BMI ≤30) (n=9 patients).

(B) Western blot analysis of α1AMPK in human granulosa cells retrieved from control or PCOS patients. Vinculin was used as control. Quantification of total α1AMPK was shown below the Western blot. (n = 6 different patient per group). The results are means ± SEM *P <0.05, **P<0.01.

Figure 11. **Consequence of α1AMPK deficiency in granulosa cells**: schematic summary of the consequences on cell metabolism, steroid production and cell proliferation.

Supplemental data 1. **Apoptosis marker in KO-KGN (A)** Quantification of the caspase-3/7 cleaved activity in KGN (n = 6 independent experiments). **(B)** P53 positive cells analyzed by High Content Screening, nutlin 5μM was used as a positive control to stabilize p53 content **(C)** Western blot analysis of β catenin in KGN granulosa cells. Results are representative of 3 independent experiments. **(D)** Immunostaining and quantification of β catenin in KGN cells. Quantification of intensity was performed by ImageJ software. Results are representative of 3

independent experiments with at least 100 cells counted per experiment. Values are the mean ± SEM.

Supplemental data 2. **Oxidative stress in KO-KGN**. **(A)** ROS content in KO-KGN and Scr-KGN cells (n = 4 independent experiments). **(B)** The intensity of the oxidative stress staining (Cellrox dye) in each cell was quantified by High Content Screening. Representative fields of Cellrox staining and a DAPI staining are represented below. Results are representative of 3 independent experiments.

Supplemental Figure 3. volcano plot of -log10 representing the RNA seq data

Supplemental data 4. RT-PCR for significant DEGs

Bar graphs show the results of a qRT-PCR validation of the mRNA-SEQ analysis using Scr-KGN and KO-KGN cells **(A)** for 3up-regulatedp-regulated (SOD2, Pentraxin, IL6) and **(B)** 3 down-regulated (COLL4a6, MMP11, CKB) differentially expressed genes.

Supplemental data 5. **Table. Comparison of DEGs with genes or proteins identifying as differentially expressed in PCOS women.**

Differentially regulated genes in KO-KGN cells were compared to genes or proteins present in a curated PCOS database ("PCOSbase" (http://pcosbase.org) (Afiqah-Aleng *et al.*, 2017). Forty-two down-regulated and 14 up-regulated genes in KO-KGN cells were also found in the PCOSbase database providing support for considering these genes as dysregulated in PCOS

827 women**.** These 56 genes are involved in cytoskeleton reorganization, metabolism, lipid
828 metabolism, and immunity.

829

830 **Supplemental data 6. BrDU assay performed on human primary granulosa-lutein cells**
831 **exposed to AMPK inhibitors.** 20.000 cells/well were seeded and were exposed for 48h to
832 AMPK inhibitor (Compound C and/or SBI-0206965). During the last 24h. cells were exposed
833 to a pulse of BrDU (24h) (n=4). One-way ANOVA was performed with Dunnett post-hoc
834 comparisons tests.

835

836 **Supplemental Figure 7. Gene expression performed on human primary granulosa-lutein**
837 **cells exposed to AMPK inhibitor (Compound C) for 24hours (n=5).**

838

839 **Supplemental Figure 8. Expression of constitutively active AMPK rescues the KO-KGN**
840 **deficient cells.** Gene expression performed on control KGN cells (KGN WT) . KO-KGN
841 cells. and KO-KGN cells infected with an adenoviral construct encoding a constitutively
842 active (CA-AMPK) (AdenoCA-AMPK-KO-KGN cells) for 48hours (n=3).

843

844 **Supplemental Figure 9. Representative picture of atretic and healthy follicle** . *: pyknotic
845 cells in atretic follicle ; h: healthy follicle. Bar. 100 µm.

846

847 **Table 1. Primers for quantitative Real-Time PCR**

Name.	Accession no	Forward primer	Reverse primer
α1AMPK	NM_006251.6	TGCGTGTACGAAGGAAGAATCC	TGTGACTTCCAGGTCTTGGAGT
α2AMPK	NM_006252.4	GGGTGAAGATCGGACACTACGT	TTGATGTTCAATCTTCACTTTG
interleukin 6 (IL6)	NM_001318095.2	CCAGCTATGAACTCCTTCTC	GCTTGTTCCTCACATCTCTC
superoxide dismutase 2 (SOD2)	NM_001322819.2	GACAAACCTCAGCCCTAACG	GAAACCAAGCCAACCCCAAC
Pentraxin 3	NM_002852.4	CGG TGC TAG AGG AGC TG	TAGCTGTTTCACAACCT
Collagen type IV alpha 6 chain (COLL4a6)	NM_001847	CACTATGCCAGGCGCAATG	CACACACAGAGCAGCGGCT
Matrix metallopeptidase 11 (MMP11)	NM_005940.5	ATTTGGTTCTTCCAAGGTGCTCAGT	CCTCGGAAGAAGTAGATCTTGTTCT
Creatine kinase (CKB)	NM_001823	GCC TCA CTC AGA TCG AAA CTC	GGC ATG TGA GGA TGT AGC CC
Actin Beta (ACTB)	NM_001101.5	ACGGAACCACAGTTTATCATC	GTCCCAGTCTTCAACTATACC
Eukaryotic Translation Elongation Factor 1 Alpha 1 (EEF1A1)	NM_001402.6	AGCAGACTTTGTGACCTTGCC	TCACATGAGACAGACGGTTGC

Glyceraldehyde -3-Phosphate Dehydrogenase (GAPDH)	NM_002046.7	ACGGATTTGGTCGTATTGGG	TGATTTTGGAGGATCTCGC

848

849

850

851 **Table 2. Biological parameters of patients from control and PCOS groups.**

852 Data are expressed as mean ± S.E.M. (range)

853

	Control (n=8)	PCOS (n=9)	p
Age	30,63±1,48 (26 - 37)	29,56±1,26 (22 - 34)	NS
BMI	21,90±0,83 (19 - 25)	20,43±0,70 (18 - 25)	NS
Testosterone (mmol/L)	1,39±0,57 (0 - 5)	4,11±1,48 (1 - 15)	<0.05
AMH (ng/mL)	3.03±0,74 (1 - 7)	22,45±6,02 (7 - 60)	<0.0001
FSH (UI/L)	7,38±1,33 (3 - 15)	5,76±0,35 (3 - 7)	NS
LH (UI/L)	4.41±0.32 (3 - 6)	8.73±1.44 (4 - 15)	<0.05
E2 (ng/l)	40.74±5.56 (25 - 73)	46.01±4.33 (32 - 72)	N.S.
Cycle duration (days)	28.25±0.87 (26 - 34)	105.06±23.86 (31 - 180)	<0.001
number of total follicles (determined by ultrasound using Rotterdam criteria)	16.25±1.94 (7 - 22)	51.00±5.86 (40 - 80)	<0.001
number of mature oocytes retrieved	4.50±0.71 (2 - 7)	7.67±1.71 (3 - 16)	N.S.

854

Supplemental data 5.

Table with Genes down-regulated in AMPK KO granulosa cells and cited in PCOSbase

protein name	gene_short_name	Log2 (FC)	p-adj	references
Associated to cytoskeleton reorganization				
collagen type IV alpha 6 chain	COL4A6	-2,811093816	6,41E-05	(Jansen *et al.*, 2004)
CXADR Ig-like cell adhesion molecule	CXADR	-2,22068001	0,003665591	(Wood *et al.*, 2005)
matrix metallopeptidase 11	MMP11	-2,191714855	0,002366685	(Oksjoki *et al.*, 2005)
collagen type IV alpha 3 chain	COL4A3	-1,812889506	0,01676443	(Wood *et al.*, 2003)
CD9 molecule	CD9	-0,938283962	0,015877884	(Oksjoki *et al.*, 2005)
lamin A/C	LMNA	-0,909314928	0,00524773	(Ma *et al.*, 2007)
formin 2	FMN2	-0,787480608	0,009844453	(Wood *et al.*, 2007)
spectrin repeat containing nuclear envelope	SYNE2	-0,783093104	0,006783443	(Diao *et al.*, 2004)
destrin, actin-depolymerizing factor	DSTN	-0,590541073	0,030849344	(Wood *et al.*, 2007)
S100 calcium-binding protein A4	S100A4	-1,895067365	1,57E-05	(Jansen *et al.*, 2004)
slit guidance ligand 2	SLIT2	-1,329733708	0,033698713	(Jansen *et al.*, 2004)
fascin actin-bundling protein 1	FSCN1	-1,238972477	0,02454077	(Jansen *et al.*, 2004)
secreted protein acidic and cysteine-rich	SPARC	-1,145819126	3,12E-09	(Diao *et al.*, 2004)
Associated to metabolism				
pyruvate dehydrogenase kinase 4	PDK4	-2,02806644	4,28E-07	(Diao *et al.*, 2004)
creatine kinase B	C.K.B.CKB	-1,821744257	0,000807503	(Jansen *et al.*, 2004)
ectonucleotide	ENPP1	-1,435662986	0,002736008	(Cortón *et al.*, 2007)
natriuretic peptide receptor 3	NPR3	-1,40238276	0,024227079	(Wood *et al.*, 2003)
ATPase Na+/K+ transporting subunit beta 1	ATP1B1	-0,944986551	0,000111989	(Jansen *et al.*, 2004)
dimethylarginine dimethylaminohydrolase 1	DDAH1	-0,690831339	0,017201613	(Ma *et al.*, 2007)
transaldolase 1	TALDO1	-0,625534732	0,002736008	(Ma *et al.*, 2007)
malate dehydrogenase 2	MDH2	-0,528110753	0,036138334	(Ma *et al.*, 2007)
membrane bound O-acyltransferase domain	MBOAT2	-0,497114539	0,032578793	(Jansen *et al.*, 2004)
Associated to lipid process				
epoxide hydrolase 1	EPHX1	-1,100535918	5,50E-09	(Wood *et al.*, 2003)
carnitine palmitoyltransferase 1A	CPT1A	-1,075237703	7,29E-06	(Ma *et al.*, 2007)
peroxisoproliferator-activatedted receptor	PPARG	-0,97258565	0,03948827	(Jansen *et al.*, 2004)
neurolysin	NLN	-0,80427469	0,036457112	(Wood *et al.*, 2007)
carnitine O-acetyltransferase	CRAT	-0,530129098	0,011647709	(Wood *et al.*, 2005)
enoyl-CoA delta isomerase 2	ECI2	-0,44686918	0,031734107	(Wood *et al.*, 2003)
others process				
major histocompatibility complex, class II,	HLA-DMB	-1,596002075	0,047066826	(Jansen *et al.*, 2004)
major histocompatibility complex, class II,	HLA-DRB1	-1,558923538	0,043282009	(Jansen *et al.*, 2004)
regulator of G protein signaling 4	RGS4	-2,097673072	1,77E-05	(Cortón *et al.*, 2007)
inhibitor of D.N.A.DNA binding 4,	ID4	-1,683876121	3,97E-09	(Wood *et al.*, 2005)
MIF4G domain containing	MIF4GD	-0,781064095	0,034780635	(Jansen *et al.*, 2004)
protein disulfide isomerase family A member	PDIA5	-0,719190616	0,000921574	(Skov *et al.*, 2007)
androgen receptor	AR	-0,692728486	0,033652953	(Panda *et al.*, 2016)
annexin A2	ANXA2	-0,677664138	0,00857582	(Ma *et al.*, 2007)
inositol-tetrakisphosphate 1-kinase	ITPK1	-0,672853363	0,011259896	(Jansen *et al.*, 2004)
adenosylhomocysteinase like 1	AHCYL1	-0,668608252	0,022208827	(Wood *et al.*, 2007)
down-regulator of transcription 1	DR1	-0,546407083	0,019436969	(Wood *et al.*, 2007)
transforming acidic coiled-coil containing	TACC1	-0,522493788	0,041172734	(Wood *et al.*, 2007)
N(alpha)-acetyltransferase 50, NatE catalytic	NAA50	-0,50865998	0,041238754	(Wood *et al.*, 2007)
chaperonin containing TCP1 subunit 3	CCT3	-0,49373307	0,023886345	(Ma *et al.*, 2007)

860 **Table with Genes up-regulated in AMPK KO granulosa cells and cited in PCOSbase**

protein name	gene_short_name	Log2 (FC) (in KO compared to control)	p-adj	references
Associated to immunity process				
caspase 4	CASP4	0,621825878	0,00940265	(Wood *et al.*, 2005) (Zafari Zangeneh *et al.*, 2017)
interleukin 1 alpha	IL1A	1,769217139	0,01499045	
interleukin 6	IL6	2,144628118	8,78E-05	(Adams *et al.*, 2016)
C-X-C motif chemokine ligand 1	CXCL1	2,551937289	7,29E-06	(Adams *et al.*, 2016)
serpin family B member 2	SERPINB2	2,723673809	6,14E-06	(Adams *et al.*, 2016)
C-C motif chemokine ligand 20	CCL20	2,830678569	1,59E-10	(Adams *et al.*, 2016)
interleukin 1 beta	IL1B	3,43972107	2,69E-13	(Zafari Zangeneh *et al.*, 2017)
expression of genes required for cumulus cell expansion				
prostaglandin-endoperoxide synthase 2	PTGS2	1,698028668	0,00678344	(Schmidt *et al.*, 2014)
pentraxin 3	PTX3	1,921101334	0,00054765	(Jin *et al.*, 2020)
others process				
activin A receptor type 1B	ACVR1B	0,523757312	0,00738568	(Panda *et al.*, 2016)
follistatin	FST	0,865977418	0,01879147	(Norman *et al.*, 2001)
cytohesin 2	CYTH2	1,053382964	0,00664545	(Oksjoki *et al.*, 2005)
superoxide dismutase 2	SOD2	1,164536069	0,02350078	(Borro *et al.*, 2007)
Uncoupling protein 3	UCP3	1,412930247	0,03166918	(Panda *et al.*, 2016)

861

862

References

Abbott DH, Dumesic DA, Levine JE. Hyperandrogenic origins of polycystic ovary syndrome - implications for pathophysiology and therapy. *Expert Rev Endocrinol Metab* 2019;**14**:131–143.

Abdalla MA, Deshmukh H, Atkin S, Sathyapalan T. A review of therapeutic options for managing the metabolic aspects of polycystic ovary syndrome. *Ther Adv Endocrinol Metab* 2020;**11**:2042018820938305.

Adams J, Liu Z, Ren YA, Wun W-S, Zhou W, Kenigsberg S, Librach C, Valdes C, Gibbons W, Richards J. Enhanced Inflammatory Transcriptome in the Granulosa Cells of Women With Polycystic Ovarian Syndrome. *J Clin Endocrinol Metab* 2016;**101**:3459–3468.

Afiqah-Aleng N, Harun S, A-Rahman MRA, Nor Muhammad NA, Mohamed-Hussein Z-A. PCOSBase: a manually curated database of polycystic ovarian syndrome. *Database (Oxford)* 2017;**2017**:bax098.

Attia GR, Rainey WE, Carr BR. Metformin directly inhibits androgen production in human thecal cells. *Fertil Steril* 2001;**76**:517–524.

Baufeld A, Koczan D, Vanselow J. Induction of altered gene expression profiles in cultured bovine granulosa cells at high cell density. *Reprod Biol Endocrinol* 2017;**15**:3.

Bertoldo MJ, Faure M, Dupont J, Froment P. Impact of metformin on reproductive tissues: an overview from gametogenesis to gestation. *Ann Transl Med* 2014;**2**:55.

Bertoldo MJ, Guibert E, Faure M, Ramé C, Foretz M, Viollet B, Dupont J, Froment P. Specific deletion of AMP-activated protein kinase (α1AMPK) in murine oocytes alters junctional protein expression and mitochondrial physiology. *PLoS ONE* 2015;**10**:e0119680.

887 Borro M, Gentile G, Stigliano A, Misiti S, Toscano V, Simmaco M. Proteomic analysis of peripheral T
888 lymphocytes, suitable circulating biosensors of strictly related diseases. *Clin Exp Immunol*
889 2007;**150**:494–501.
890 Bowdridge EC, Goravanahally MP, Inskeep EK, Flores JA. Activation of Adenosine Monophosphate-
891 Activated Protein Kinase Is an Additional Mechanism That Participates in Mediating
892 Inhibitory Actions of Prostaglandin F2Alpha in Mature, but Not Developing, Bovine Corpora
893 Lutea. *Biol Reprod* 2015;**93**:7.
894 Bowdridge EC, Vernon MW, Flores JA, Clemmer MJ. In vitro progesterone production by luteinized
895 human mural granulosa cells is modulated by activation of AMPK and cause of infertility.
896 *Reprod Biol Endocrinol* 2017;**15**:76.
897 Buresova J, Janovska P, Kuda O, Krizova J, Stelt IR der, Keijer J, Hansikova H, Rossmeisl M, Kopecky J.
898 Postnatal induction of muscle fatty acid oxidation in mice differing in propensity to obesity: a
899 role of pyruvate dehydrogenase. *Int J Obes (Lond)* 2020;**44**:235–244.
900 Caldwell ASL, Middleton LJ, Jimenez M, Desai R, McMahon AC, Allan CM, Handelsman DJ, Walters KA.
901 Characterization of reproductive, metabolic, and endocrine features of polycystic ovary
902 syndrome in female hyperandrogenic mouse models. *Endocrinology* 2014;**155**:3146–3159.
903 Controlling the False Discovery Rate: A Practical and Powerful Approach to Multiple Testing *J Roy Stat*
904 *Soc Series B* 1995;**57**:289–300.
905 Cortón M, Botella-Carretero JI, Benguría A, Villuendas G, Zaballos A, San Millán JL, Escobar-Morreale
906 HF, Peral B. Differential gene expression profile in omental adipose tissue in women with
907 polycystic ovary syndrome. *J Clin Endocrinol Metab* 2007;**92**:328–337.
908 Diao F-Y, Xu M, Hu Y, Li J, Xu Z, Lin M, Wang L, Zhou Y, Zhou Z, Liu J, *et al.* The molecular
909 characteristics of polycystic ovary syndrome (PCOS) ovary defined by human ovary cDNA
910 microarray. *J Mol Endocrinol* 2004;**33**:59–72.
911 Downs SM, Mastropolo AM. The participation of energy substrates in the control of meiotic
912 maturation in murine oocytes. *Dev Biol* 1994;**162**:154–168.

913 Downs SM, Ya R, Davis CC. Role of AMPK throughout meiotic maturation in the mouse oocyte:
914 evidence for promotion of polar body formation and suppression of premature activation.
915 *Mol Reprod Dev* 2010;**77**:888–899.
916 Dupont J, Reverchon M, Cloix L, Froment P, Ramé C. Involvement of adipokines, AMPK, PI3K and the
917 PPAR signaling pathways in ovarian follicle development and cancer. *Int J Dev Biol*
918 2012;**56**:959–967.
919 Ehrmann DA, Liljenquist DR, Kasza K, Azziz R, Legro RS, Ghazzi MN, PCOS/Troglitazone Study Group.
920 Prevalence and predictors of the metabolic syndrome in women with polycystic ovary
921 syndrome. *J Clin Endocrinol Metab* 2006;**91**:48–53.
922 El Hayek S, Bitar L, Hamdar LH, Mirza FG, Daoud G. Poly Cystic Ovarian Syndrome: An Updated
923 Overview. *Front Physiol* 2016;**7**:124.
924 Estienne A, Bongrani A, Reverchon M, Ramé C, Ducluzeau P-H, Froment P, Dupont J. Involvement of
925 Novel Adipokines, Chemerin, Visfatin, Resistin and Apelin in Reproductive Functions in
926 Normal and Pathological Conditions in Humans and Animal Models. *Int J Mol Sci* 2019;**20**:.
927 Faubert B, Vincent EE, Poffenberger MC, Jones RG. The AMP-activated protein kinase (AMPK) and
928 cancer: many faces of a metabolic regulator. *Cancer Lett* 2015;**356**:165–170.
929 Faure M, Bertoldo MJ, Khoueiry R, Bongrani A, Brion F, Giulivi C, Dupont J, Froment P. Metformin in
930 Reproductive Biology. *Front Endocrinol (Lausanne)* 2018;**9**:675.
931 Franks S, Stark J, Hardy K. Follicle dynamics and anovulation in polycystic ovary syndrome. *Hum*
932 *Reprod Update* 2008;**14**:367–378.
933 Franz MB, Daube S, Keck C, Sator M, Pietrowski D. Small GTPases are involved in sprout formation in
934 human granulosa lutein cells. *Arch Gynecol Obstet* 2013;**287**:819–824.
935 Fulghesu AM, Romualdi D, Di Florio C, Sanna S, Tagliaferri V, Gambineri A, Tomassoni F, Minerba L,
936 Pasquali R, Lanzone A. Is there a dose-response relationship of metformin treatment in
937 patients with polycystic ovary syndrome? Results from a multicentric study. *Hum Reprod*
938 2012;**27**:3057–3066.

939 Furat Rencber S, Kurnaz Ozbek S, Eraldemır C, Sezer Z, Kum T, Ceylan S, Guzel E. Effect of resveratrol
940 and metformin on ovarian reserve and ultrastructure in PCOS: an experimental study. *J*
941 *Ovarian Res* 2018;**11**:55.
942 Ghillebert R, Swinnen E, Wen J, Vandesteene L, Ramon M, Norga K, Rolland F, Winderickx J. The
943 AMPK/SNF1/SnRK1 fuel gauge and energy regulator: structure, function and regulation. *FEBS*
944 *J* 2011;**278**:3978–3990.
945 Grenier A, Sujobert P, Olivier S, Guermouche H, Mondésir J, Kosmider O, Viollet B, Tamburini J.
946 Knockdown of Human AMPK Using the CRISPR/Cas9 Genome-Editing System. *Methods Mol*
947 *Biol* 2018;**1732**:171–194.
948 Guévélou E, Huvet A, Galindo-Sánchez CE, Milan M, Quillien V, Daniel J-Y, Quéré C, Boudry P,
949 Corporeau C. Sex-specific regulation of AMP-activated protein kinase (AMPK) in the Pacific
950 oyster Crassostrea gigas. *Biol Reprod* 2013;**89**:100.
951 Hardie DG, Schaffer BE, Brunet A. AMPK: An Energy-Sensing Pathway with Multiple Inputs and
952 Outputs. *Trends Cell Biol* 2016;**26**:190–201.
953 Hardie DG, Scott JW, Pan DA, Hudson ER. Management of cellular energy by the AMP-activated
954 protein kinase system. *FEBS Lett* 2003;**546**:113–120.
955 Houten SM, Chegary M, Te Brinke H, Wijnen WJ, Glatz JFC, Luiken JJFP, Wijburg FA, Wanders RJA.
956 Pyruvate dehydrogenase kinase 4 expression is synergistically induced by AMP-activated
957 protein kinase and fatty acids. *Cell Mol Life Sci* 2009;**66**:1283–1294.
958 Jansen E, Laven JSE, Dommerholt HBR, Polman J, Rijt C van, Hurk C van den, Westland J, Mosselman
959 S, Fauser BCJM. Abnormal gene expression profiles in human ovaries from polycystic ovary
960 syndrome patients. *Mol Endocrinol* 2004;**18**:3050–3063.
961 Jiang Z-Z, Hu M-W, Ma X-S, Schatten H, Fan H-Y, Wang Z-B, Sun Q-Y. LKB1 acts as a critical gatekeeper
962 of ovarian primordial follicle pool. *Oncotarget* 2016;**7**:5738–5753.

963 Jin J, Ma Y, Tong X, Yang W, Dai Y, Pan Y, Ren P, Liu L, Fan H-Y, Zhang Y, *et al.* Metformin inhibits
964 testosterone-induced endoplasmic reticulum stress in ovarian granulosa cells via inactivation
965 of p38 MAPK. *Hum Reprod* 2020;**35**:1145–1158.
966 Joham AE, Teede HJ, Ranasinha S, Zoungas S, Boyle J. Prevalence of infertility and use of fertility
967 treatment in women with polycystic ovary syndrome: data from a large community-based
968 cohort study. *J Womens Health (Larchmt)* 2015;**24**:299–307.
969 Jørgensen SB, Viollet B, Andreelli F, Frøsig C, Birk JB, Schjerling P, Vaulont S, Richter EA, Wojtaszewski
970 JFP. Knockout of the alpha2 but not alpha1 5'-AMP-activated protein kinase isoform
971 abolishes 5-aminoimidazole-4-carboxamide-1-beta-4-ribofuranosidebut not contraction-
972 induced glucose uptake in skeletal muscle. *J Biol Chem* 2004;**279**:1070–1079.
973 Klein DK, Pilegaard H, Treebak JT, Jensen TE, Viollet B, Schjerling P, Wojtaszewski JFP. Lack of
974 AMPKalpha2 enhances pyruvate dehydrogenase activity during exercise. *Am J Physiol*
975 *Endocrinol Metab* 2007;**293**:E1242-1249.
976 Le Bellego F, Fabre S, Pisselet C, Monniaux D. Cytoskeleton reorganization mediates alpha6beta1
977 integrin-associated actions of laminin on proliferation and survival, but not on
978 steroidogenesis of ovine granulosa cells. *Reprod Biol Endocrinol* 2005;**3**:19.
979 Lee S-H, Chung D-J, Lee H-S, Kim T-J, Kim M-H, Jeong HJ, Im J-A, Lee D-C, Lee J-W. Mitochondrial DNA
980 copy number in peripheral blood in polycystic ovary syndrome. *Metabolism* 2011;**60**:1677–
981 1682.
982 Love MI, Huber W, Anders S. Moderated estimation of fold change and dispersion for RNA-seq data
983 with DESeq2. *Genome Biol* 2014;**15**:550.
984 Ma X, Fan L, Meng Y, Hou Z, Mao Y-D, Wang W, Ding W, Liu J-Y. Proteomic analysis of human ovaries
985 from normal and polycystic ovarian syndrome. *Mol Hum Reprod* 2007;**13**:527–535.
986 Mansfield R, Galea R, Brincat M, Hole D, Mason H. Metformin has direct effects on human ovarian
987 steroidogenesis. *Fertil Steril* 2003;**79**:956–962.

988 Mayes MA, Laforest MF, Guillemette C, Gilchrist RB, Richard FJ. Adenosine 5'-monophosphate
989 kinase-activated protein kinase (PRKA) activators delay meiotic resumption in porcine
990 oocytes. *Biol Reprod* 2007;**76**:589–597.
991 Meunier C, Blondelle D, Faure P, Baguet J-P, Le Goff C, Chabre O, Ducros V. Development and
992 validation of a method using supported liquid extraction for aldosterone determination in
993 human plasma by LC-MS/MS. *Clin Chim Acta* 2015;**447**:8–15.
994 Min Z, Gao Q, Zhen X, Fan Y, Tan T, Li R, Zhao Y, Yu Y. New insights into the genic and metabolic
995 characteristics of induced pluripotent stem cells from polycystic ovary syndrome women.
996 *Stem Cell Res Ther* 2018;**9**:210.
997 Monniaux D, Genêt C, Maillard V, Jarrier P, Adriaensen H, Hennequet-Antier C, Lainé A-L, Laclie C,
998 Papillier P, Plisson-Petit F, *et al.* Prenatal programming by testosterone of follicular theca cell
999 functions in ovary. *Cell Mol Life Sci* 2020;**77**:1177–1196.
1000 Nishi Y, Yanase T, Mu Y, Oba K, Ichino I, Saito M, Nomura M, Mukasa C, Okabe T, Goto K, *et al.*
1001 Establishment and characterization of a steroidogenic human granulosa-like tumor cell line,
1002 KGN, that expresses functional follicle-stimulating hormone receptor. *Endocrinology*
1003 2001;**142**:437–445.
1004 Norman RJ, Milner CR, Groome NP, Robertson DM. Circulating follistatin concentrations are higher
1005 and activin concentrations are lower in polycystic ovarian syndrome. *Hum Reprod*
1006 2001;**16**:668–672.
1007 Oksjoki S, Söderström M, Inki P, Vuorio E, Anttila L. Molecular profiling of polycystic ovaries for
1008 markers of cell invasion and matrix turnover. *Fertil Steril* 2005;**83**:937–944.
1009 Palomba S, Orio F, Falbo A, Manguso F, Russo T, Cascella T, Tolino A, Carmina E, Colao A, Zullo F.
1010 Prospective parallel randomized, double-blind, double-dummy controlled clinical trial
1011 comparing clomiphene citrate and metformin as the first-line treatment for ovulation
1012 induction in nonobese anovulatory women with polycystic ovary syndrome. *J Clin Endocrinol*
1013 *Metab* 2005;**90**:4068–4074.

1014 Panda PK, Rane R, Ravichandran R, Singh S, Panchal H. Genetics of PCOS: A systematic bioinformatics
1015 approach to unveil the proteins responsible for PCOS. *Genom Data* 2016;**8**:52–60.
1016 Pellatt L, Rice S, Dilaver N, Heshri A, Galea R, Brincat M, Brown K, Simpson ER, Mason HD. Anti-
1017 Müllerian hormone reduces follicle sensitivity to follicle-stimulating hormone in human
1018 granulosa cells. *Fertil Steril* 2011;**96**:1246-1251.e1.
1019 Pesant M-H, Baillargeon J-P. Clinically useful predictors of conversion to abnormal glucose tolerance
1020 in women with polycystic ovary syndrome. *Fertil Steril* 2011;**95**:210–215.
1021 Roche J, Ramé C, Reverchon M, Mellouk N, Cornuau M, Guerif F, Froment P, Dupont J. Apelin (APLN)
1022 and Apelin Receptor (APLNR) in Human Ovary: Expression, Signaling, and Regulation of
1023 Steroidogenesis in Primary Human Luteinized Granulosa Cells. *Biol Reprod* 2016;**95**:104.
1024 Rodgers RJ, Irving-Rodgers HF, Wezel IL van, Krupa M, Lavranos TC. Dynamics of the membrana
1025 granulosa during expansion of the ovarian follicular antrum. *Mol Cell Endocrinol*
1026 2001;**171**:41–48.
1027 Rodriguez Paris V, Edwards MC, Aflatounian A, Bertoldo MJ, Ledger WL, Handelsman DJ, Gilchrist RB,
1028 Walters KA. Pathogenesis of Reproductive and Metabolic PCOS Traits in a Mouse Model. *J*
1029 *Endocr Soc* 2021;**5**:bvab060.
1030 Rolaki A, Coukos G, Loutradis D, DeLisser HM, Coutifaris C, Makrigiannakis A. Luteogenic hormones
1031 act through a vascular endothelial growth factor-dependent mechanism to up-regulate alpha
1032 5 beta 1 and alpha v beta 3 integrins, promoting the migration and survival of human
1033 luteinized granulosa cells. *Am J Pathol* 2007;**170**:1561–1572.
1034 Rotterdam ESHRE/ASRM-Sponsored PCOS Consensus Workshop Group. Revised 2003 consensus on
1035 diagnostic criteria and long-term health risks related to polycystic ovary syndrome. *Fertil*
1036 *Steril* 2004;**81**:19–25.
1037 Ryu Y, Kim SW, Kim YY, Ku S-Y. Animal Models for Human Polycystic Ovary Syndrome (PCOS) Focused
1038 on the Use of Indirect Hormonal Perturbations: A Review of the Literature. *Int J Mol Sci*
1039 2019;**20**:E2720.

1040 Schmidt J, Weijdegård B, Mikkelsen AL, Lindenberg S, Nilsson L, Brännström M. Differential
1041 expression of inflammation-related genes in the ovarian stroma and granulosa cells of PCOS
1042 women. *Mol Hum Reprod* 2014;**20**:49–58.
1043 Sirmans SM, Pate KA. Epidemiology, diagnosis, and management of polycystic ovary syndrome. *Clin*
1044 *Epidemiol* 2013;**6**:1–13.
1045 Skov V, Glintborg D, Knudsen S, Jensen T, Kruse TA, Tan Q, Brusgaard K, Beck-Nielsen H, Højlund K.
1046 Reduced expression of nuclear-encoded genes involved in mitochondrial oxidative
1047 metabolism in skeletal muscle of insulin-resistant women with polycystic ovary syndrome.
1048 *Diabetes* 2007;**56**:2349–2355.
1049 Stracquadanio M, Ciotta L, Palumbo MA. Relationship between serum anti-Mullerian hormone and
1050 intrafollicular AMH levels in PCOS women. *Gynecol Endocrinol* 2018;**34**:223–228.
1051 Sujobert P, Poulain L, Paubelle E, Zylbersztejn F, Grenier A, Lambert M, Townsend EC, Brusq J-M,
1052 Nicodeme E, Decrooqc J, *et al.* Co-activation of AMPK and mTORC1 Induces Cytotoxicity in
1053 Acute Myeloid Leukemia. *Cell Rep* 2015;**11**:1446–1457.
1054 Talebi R, Ahmadi A, Afraz F, Sarry J, Plisson-Petit F, Genêt C, Fabre S. Transcriptome analysis of ovine
1055 granulosa cells reveals differences between small antral follicles collected during the
1056 follicular and luteal phases. *Theriogenology* 2018;**108**:103–117.
1057 Tamura K, Makino A, Hullin-Matsuda F, Kobayashi T, Furihata M, Chung S, Ashida S, Miki T, Fujioka T,
1058 Shuin T, *et al.* Novel lipogenic enzyme ELOVL7 is involved in prostate cancer growth through
1059 saturated long-chain fatty acid metabolism. *Cancer Res* 2009;**69**:8133–8140.
1060 Tao X, Chen L, Cai L, Ge S, Deng X. Regulatory effects of the AMPKα-SIRT1 molecular pathway on
1061 insulin resistance in PCOS mice: An in vitro and in vivo study. *Biochem Biophys Res Commun*
1062 2017;**494**:615–620.
1063 Tartarin P, Guibert E, Touré A, Ouiste C, Leclerc J, Sanz N, Brière S, Dacheux J-L, Delaleu B, McNeilly
1064 JR, *et al.* Inactivation of AMPKα1 induces asthenozoospermia and alters spermatozoa
1065 morphology. *Endocrinology* 2012;**153**:3468–3481.

1066 Tata B, Mimouni NEH, Barbotin A-L, Malone SA, Loyens A, Pigny P, Dewailly D, Catteau-Jonard S,
1067 Sundström-Poromaa I, Piltonen TT, *et al.* Elevated prenatal anti-Müllerian hormone
1068 reprograms the fetus and induces polycystic ovary syndrome in adulthood. *Nat Med*
1069 2018;**24**:834–846.
1070 Teede HJ, Misso ML, Costello MF, Dokras A, Laven J, Moran L, Piltonen T, Norman RJ, International
1071 PCOS Network. Recommendations from the international evidence-based guideline for the
1072 assessment and management of polycystic ovary syndrome. *Fertil Steril* 2018;**110**:364–379.
1073 Torres-Rovira L, Gonzalez-Bulnes A, Succu S, Spezzigu A, Manca ME, Leoni GG, Sanna M, Pirino S,
1074 Gallus M, Naitana S, *et al.* Predictive value of antral follicle count and anti-Müllerian
1075 hormone for follicle and oocyte developmental competence during the early prepubertal
1076 period in a sheep model. *Reprod Fertil Dev* 2014;**26**:1094–1106.
1077 Tosca L, Chabrolle C, Uzbekova S, Dupont J. Effects of metformin on bovine granulosa cells
1078 steroidogenesis: possible involvement of adenosine 5' monophosphate-activated protein
1079 kinase (AMPK). *Biol Reprod* 2007a;**76**:368–378.
1080 Tosca L, Crochet S, Ferré P, Foufelle F, Tesseraud S, Dupont J. AMP-activated protein kinase
1081 activation modulates progesterone secretion in granulosa cells from hen preovulatory
1082 follicles. *J Endocrinol* 2006;**190**:85–97.
1083 Tosca L, Froment P, Solnais P, Ferré P, Foufelle F, Dupont J. Adenosine 5'-monophosphate-activated
1084 protein kinase regulates progesterone secretion in rat granulosa cells. *Endocrinology*
1085 2005;**146**:4500–4513.
1086 Tosca L, Ramé C, Chabrolle C, Tesseraud S, Dupont J. Metformin decreases IGF1-induced cell
1087 proliferation and protein synthesis through AMP-activated protein kinase in cultured bovine
1088 granulosa cells. *Reproduction* 2010;**139**:409–418.
1089 Tosca L, Uzbekova S, Chabrolle C, Dupont J. Possible role of 5'AMP-activated protein kinase in the
1090 metformin-mediated arrest of bovine oocytes at the germinal vesicle stage during in vitro
1091 maturation. *Biol Reprod* 2007b;**77**:452–465.

1092 Valeri C, Lovaisa MM, Racine C, Edelsztein NY, Riggio M, Giulianelli S, Venara M, Bedecarrás P,
1093 Ballerini MG, Clemente N di, *et al.* Molecular mechanisms underlying AMH elevation in
1094 hyperoestrogenic states in males. *Sci Rep* 2020;**10**:15062.
1095 Vandesompele J, De Preter K, Pattyn F, Poppe B, Van Roy N, De Paepe A, Speleman F. Accurate
1096 normalization of real-time quantitative RT-PCR data by geometric averaging of multiple
1097 internal control genes. *Genome Biol* 2002;**3**:RESEARCH0034.
1098 Varet H, Brillet-Guéguen L, Coppée J-Y, Dillies M-A. SARTools: A DESeq2- and EdgeR-Based R Pipeline
1099 for Comprehensive Differential Analysis of RNA-Seq Data. *PLoS One* 2016;**11**:e0157022.
1100 Visser JA, Jong FH de, Laven JSE, Themmen APN. Anti-Müllerian hormone: a new marker for ovarian
1101 function. *Reproduction* 2006;**131**:1–9.
1102 West ER, Shea LD, Woodruff TK. Engineering the follicle microenvironment. *Semin Reprod Med*
1103 2007;**25**:287–299.
1104 Witchel SF, Oberfield SE, Peña AS. Polycystic Ovary Syndrome: Pathophysiology, Presentation, and
1105 Treatment With Emphasis on Adolescent Girls. *J Endocr Soc* 2019;**3**:1545–1573.
1106 Wood JR, Dumesic DA, Abbott DH, Strauss JF. Molecular abnormalities in oocytes from women with
1107 polycystic ovary syndrome revealed by microarray analysis. *J Clin Endocrinol Metab*
1108 2007;**92**:705–713.
1109 Wood JR, Nelson VL, Ho C, Jansen E, Wang CY, Urbanek M, McAllister JM, Mosselman S, Strauss JF.
1110 The molecular phenotype of polycystic ovary syndrome (PCOS) theca cells and new candidate
1111 PCOS genes defined by microarray analysis. *J Biol Chem* 2003;**278**:26380–26390.
1112 Wood JR, Nelson-Degrave VL, Jansen E, McAllister JM, Mosselman S, Strauss JF. Valproate-induced
1113 alterations in human theca cell gene expression: clues to the association between valproate
1114 use and metabolic side effects. *Physiol Genomics* 2005;**20**:233–243.
1115 Wu Y, Tu M, Huang Y, Liu Y, Zhang D. Association of Metformin With Pregnancy Outcomes in Women
1116 With Polycystic Ovarian Syndrome Undergoing In Vitro Fertilization: A Systematic Review and
1117 Meta-analysis. *JAMA Netw Open* 2020;**3**:e2011995.

1118 Zafari Zangeneh F, Naghizadeh MM, Masoumi M. Polycystic ovary syndrome and circulating
1119 inflammatory markers. *Int J Reprod Biomed* 2017;**15**:375–382.
1120 Zhou Y, Zhou B, Pache L, Chang M, Khodabakhshi AH, Tanaseichuk O, Benner C, Chanda SK.
1121 Metascape provides a biologist-oriented resource for the analysis of systems-level datasets.
1122 *Nat Commun* 2019;**10**:1523.
1123

Figure 1

A

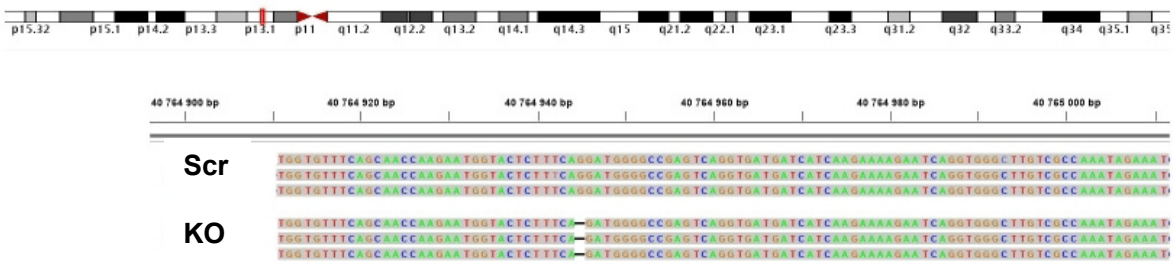
p15.32 p15.1 p14.2 p13.3 p13.1 p11 q11.2 q12.2 q13.2 q14.1 q14.3 q15 q21.2 q22.1 q23.1 q23.3 q31.2 q32 q33.2 q34 q35.1
40 764 900 bp
40 764 920 bp
40 764 940 bp
40 764 960 bp
40 764 980 bp
40 765 000 bp
Scr
KO

B

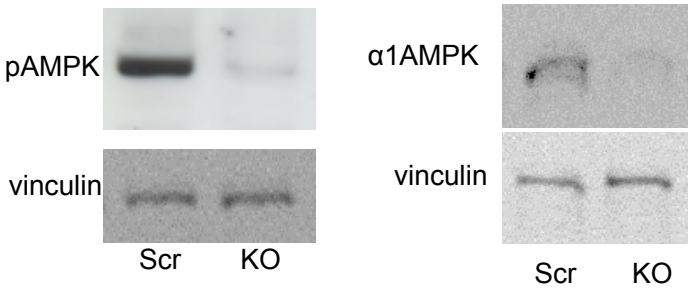
pAMPK
vinculin
Scr
KO
α1AMPK
vinculin
Scr
KO

Figure 2

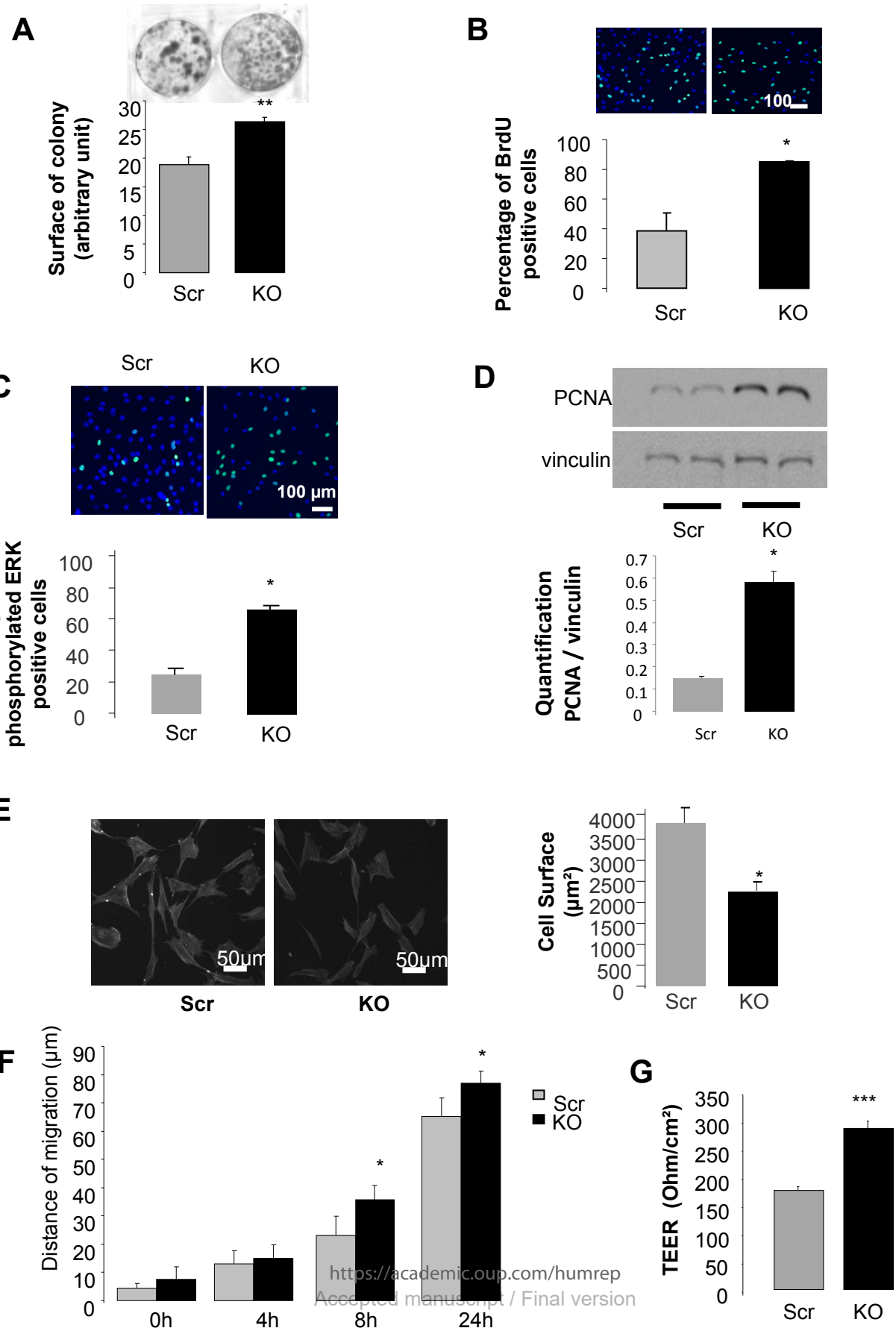

Figure 3

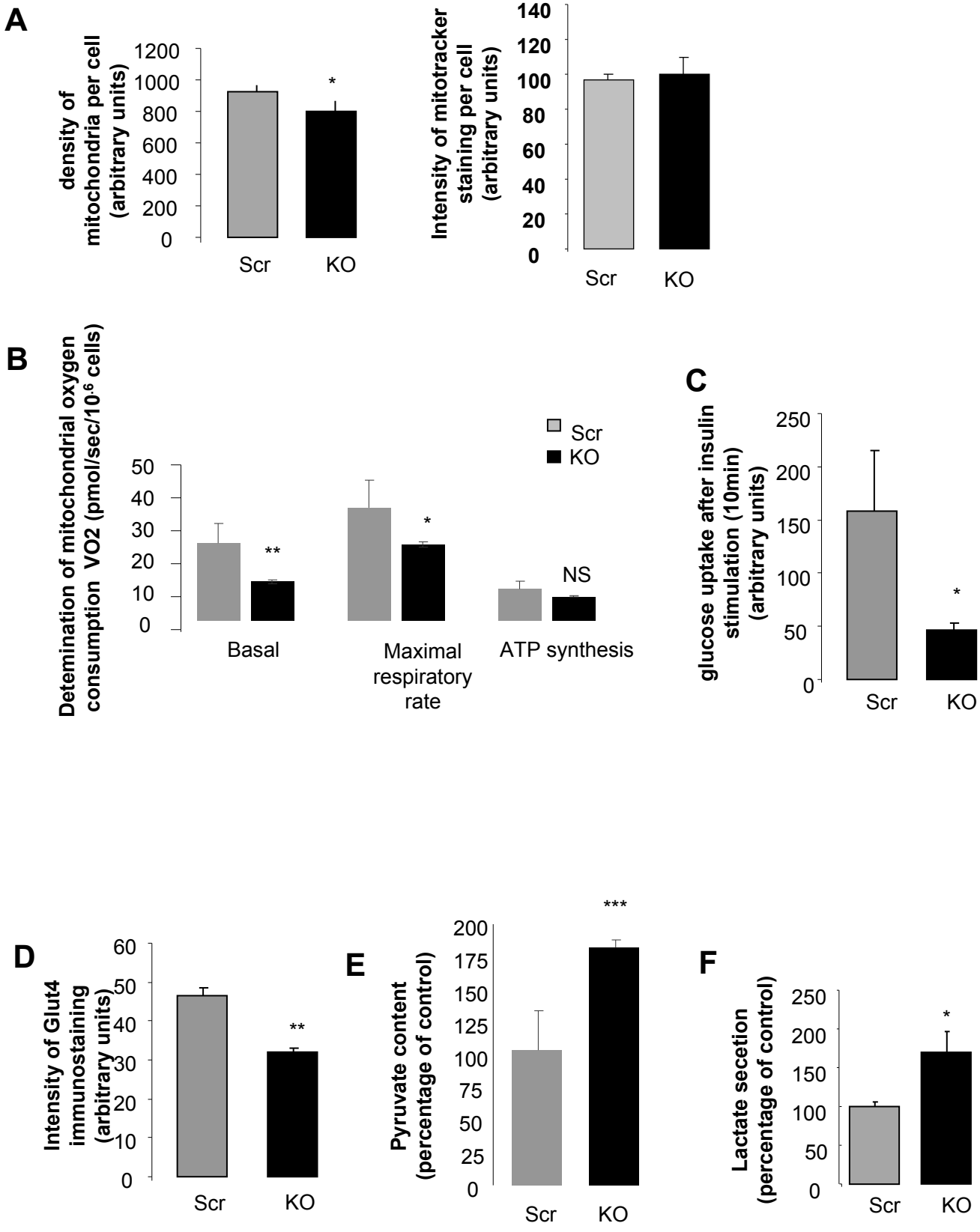
A
density of mitochondria per cell (arbitrary units)
1200
1000
800
600
400
200
0
*
Scr
KO
Intensity of mitotracker staining per cell (arbitrary units)
140
120
100
80
60
40
20
0
Scr
KO
B
Detemination of mitochondrial oxygen consumption VO2 (pmol/sec/10-6 cells)
50
40
30
20
10
0
Scr
KO
**
*
NS
Basal
Maximal respiratory rate
ATP synthesis
C
glucose uptake after insulin stimulation (10min) (arbitrary units)
250
200
150
100
50
0
*
Scr
KO
D
Intensity of Glut4 immunostaining (arbitrary units)
60
50
40
30
20
10
0
**
Scr
KO
E
Pyruvate content (percentage of control)
200
175
150
125
100
75
50
25
0
***
Scr
KO
F
Lactate secetion (percentage of control)
250
200
150
100
50
0
*
Scr
KO

Figure 4

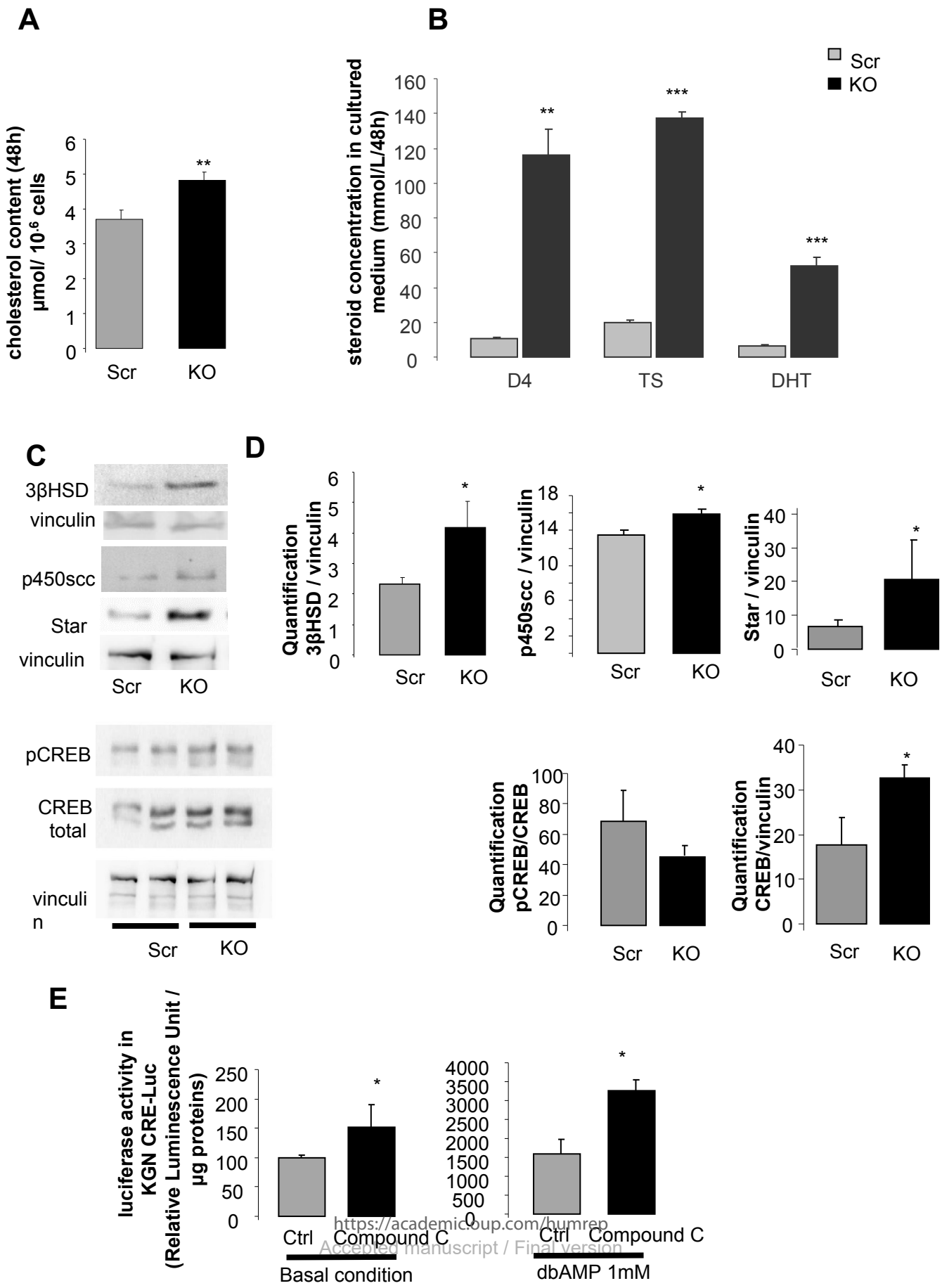

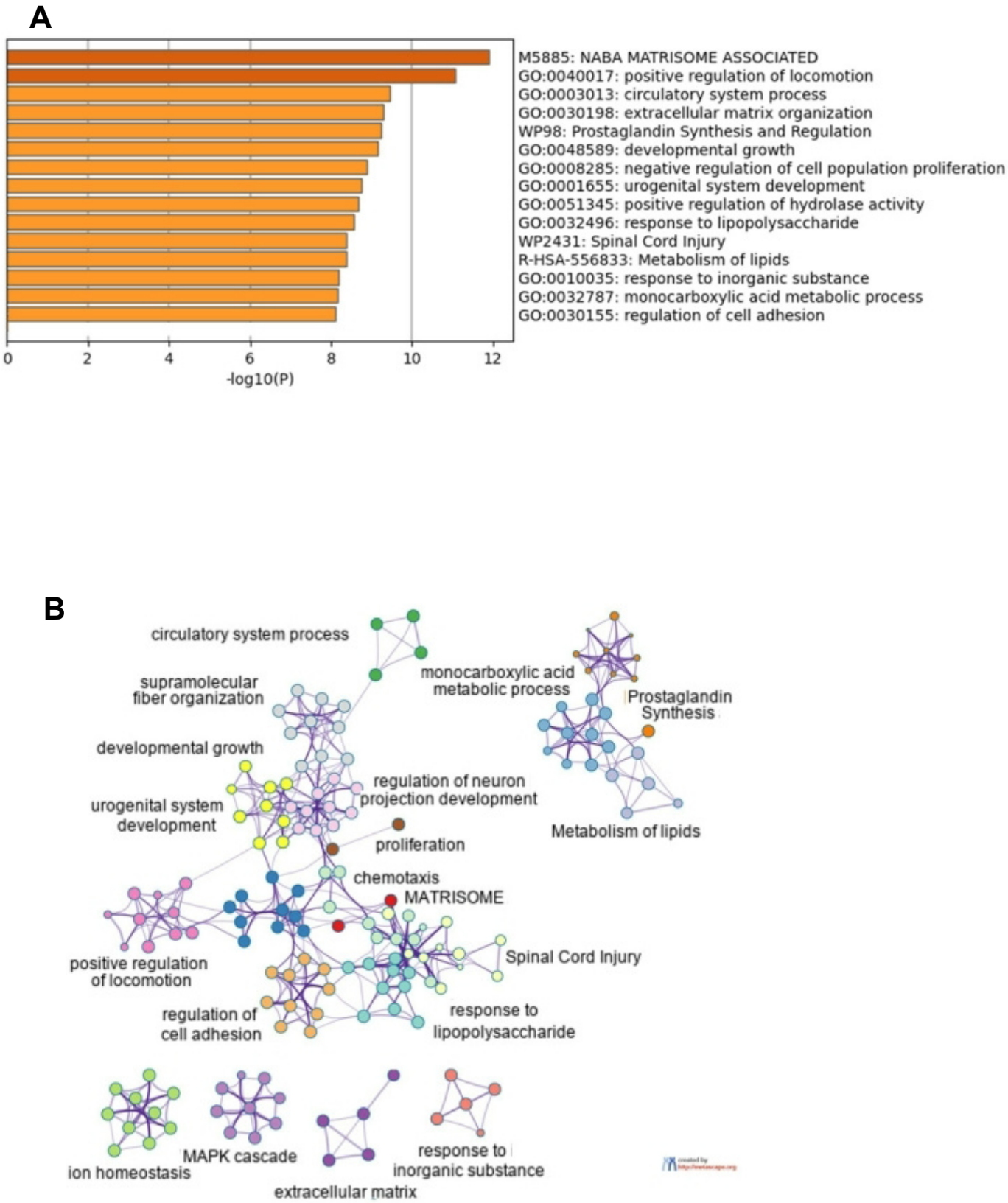
A
M5885: NABA MATRISOME ASSOCIATED
GO:0040017: positive regulation of locomotion
GO:0003013: circulatory system process
GO:0030198: extracellular matrix organization
WP98: Prostaglandin Synthesis and Regulation
GO:0048589: developmental growth
GO:0008285: negative regulation of cell population proliferation
GO:0001655: urogenital system development
GO:0051345: positive regulation of hydrolase activity
GO:0032496: response to lipopolysaccharide
WP2431: Spinal Cord Injury
R-HSA-556833: Metabolism of lipids
GO:0010035: response to inorganic substance
GO:0032787: monocarboxylic acid metabolic process
GO:0030155: regulation of cell adhesion
0
2
4
6
8
10
12
-log10(P)
B
circulatory system process
supramolecular fiber organization
developmental growth
urogenital system development
regulation of neuron projection development
proliferation
chemotaxis
MATRISOME
positive regulation of locomotion
regulation of cell adhesion
monocarboxylic acid metabolic process
Prostaglandin Synthesis
Metabolism of lipids
Spinal Cord Injury
response to lipopolysaccharide
ion homeostasis
MAPK cascade
extracellular matrix
response to inorganic substance

Figure 6

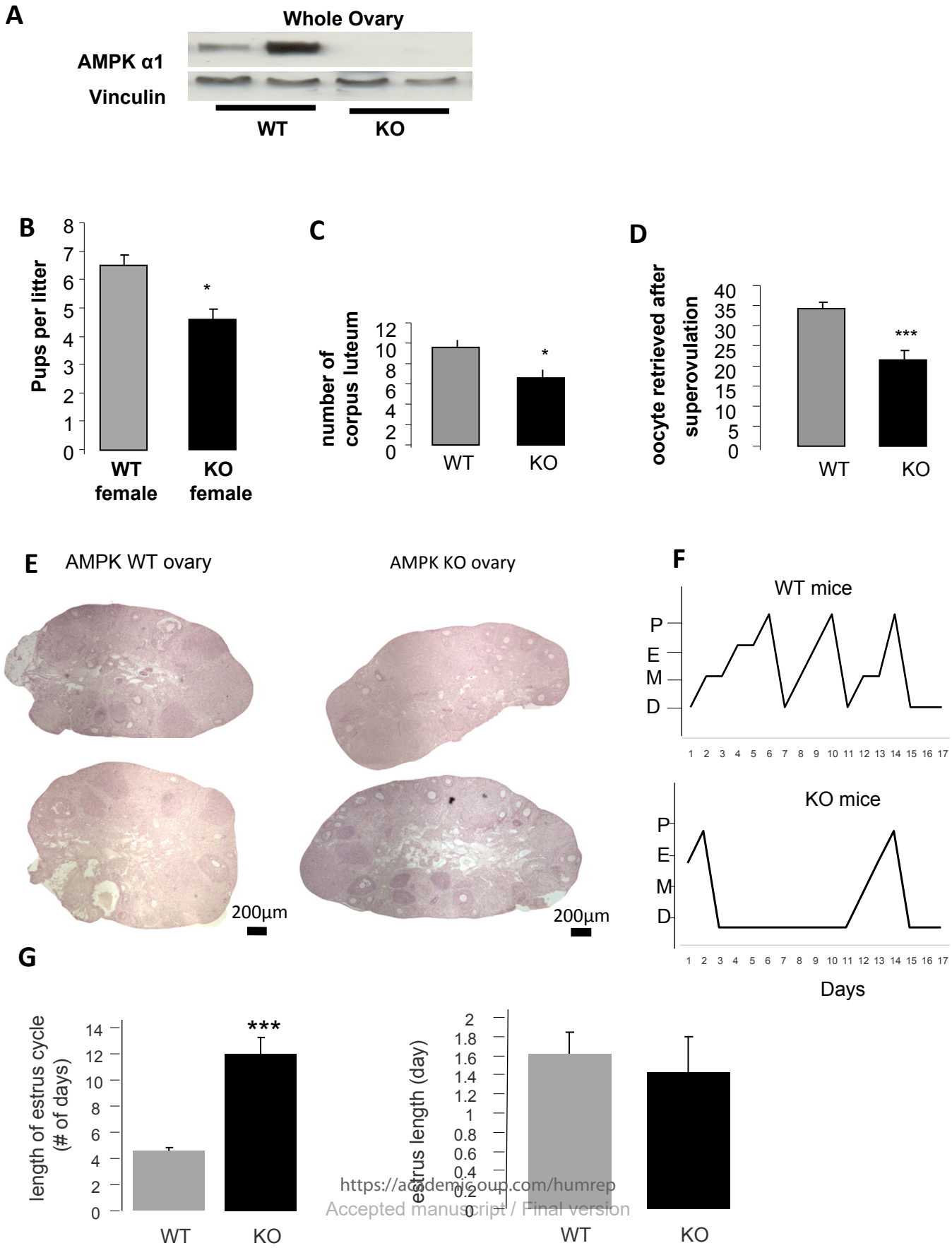

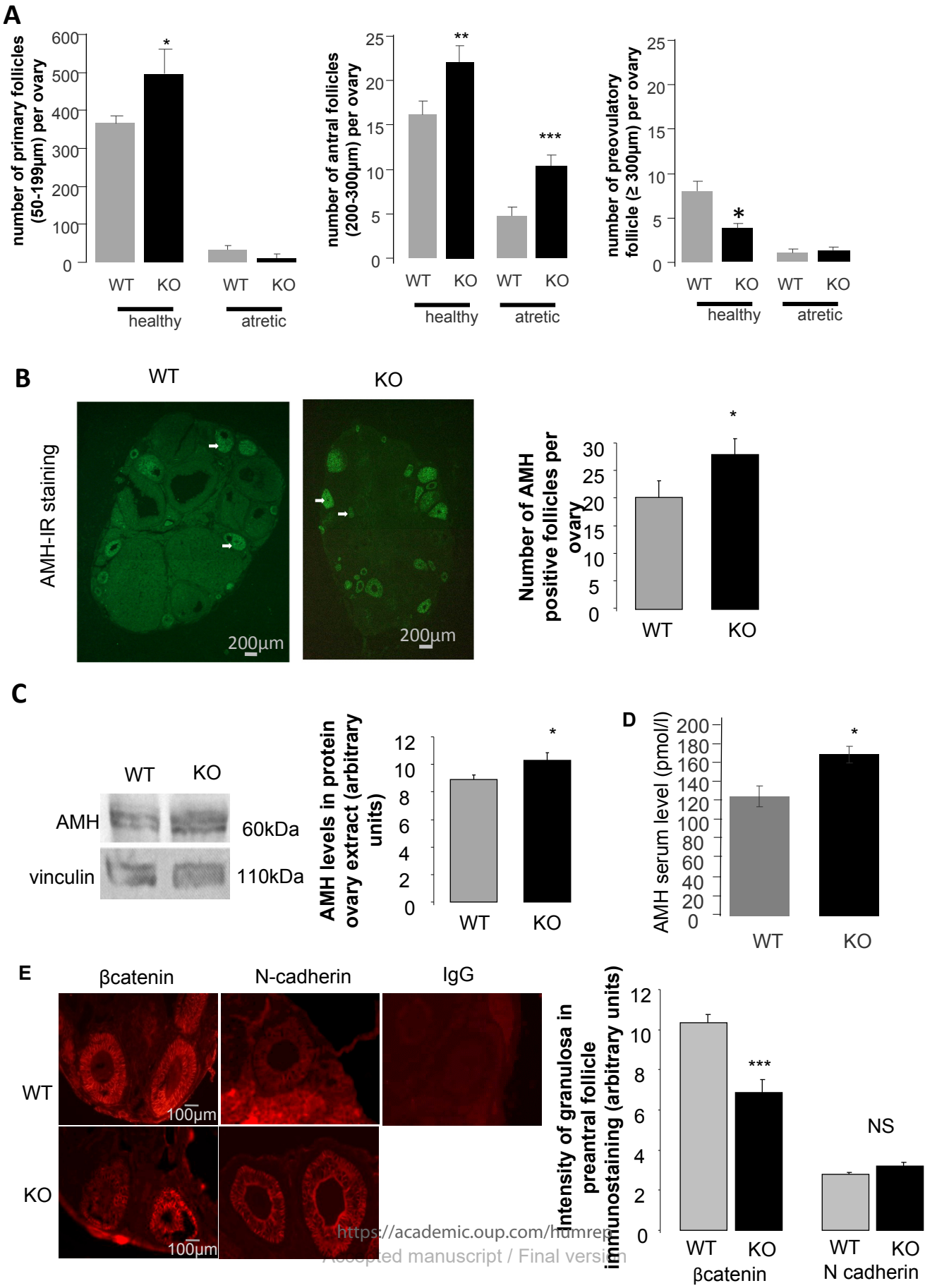

Figure 8

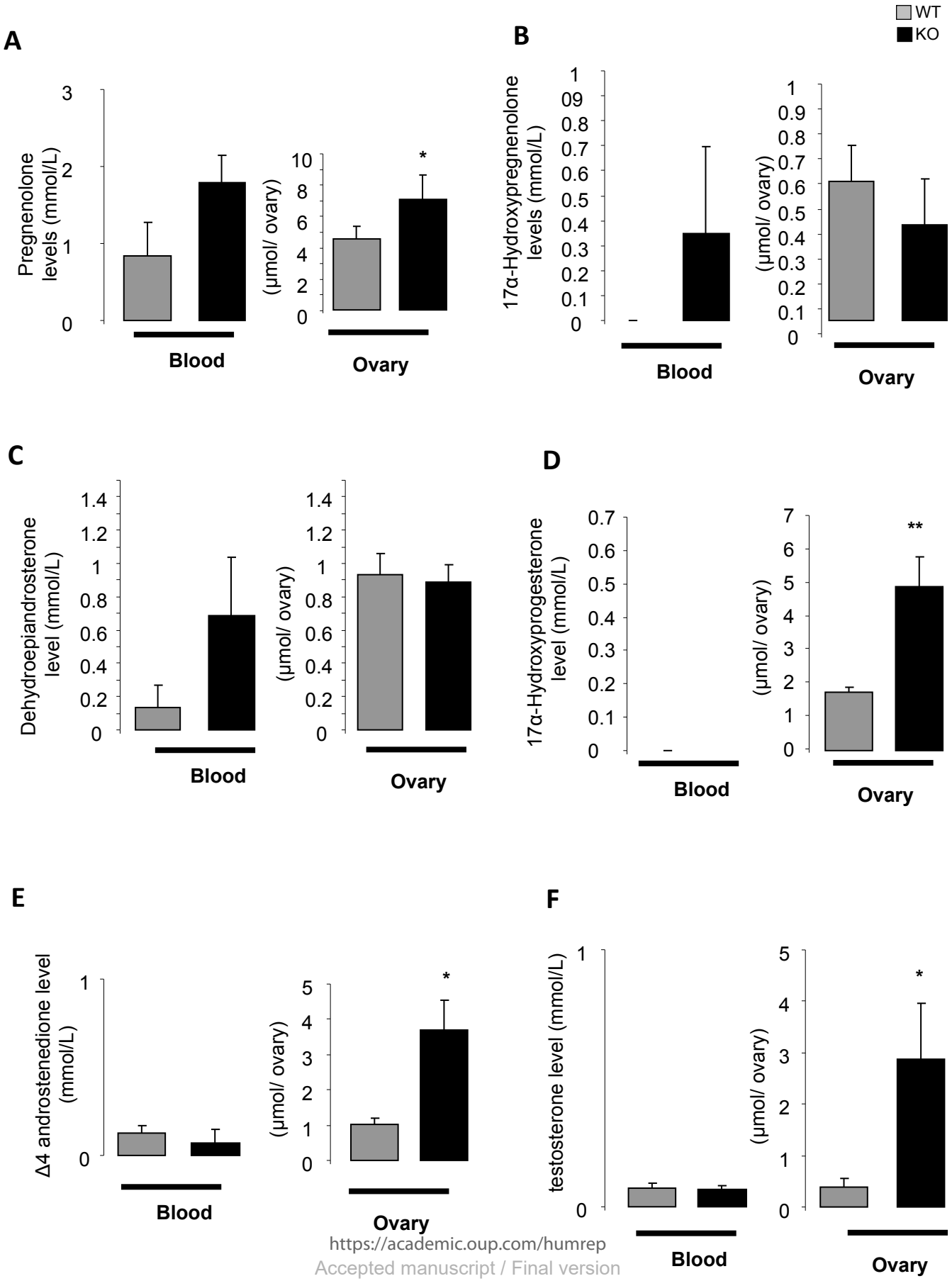

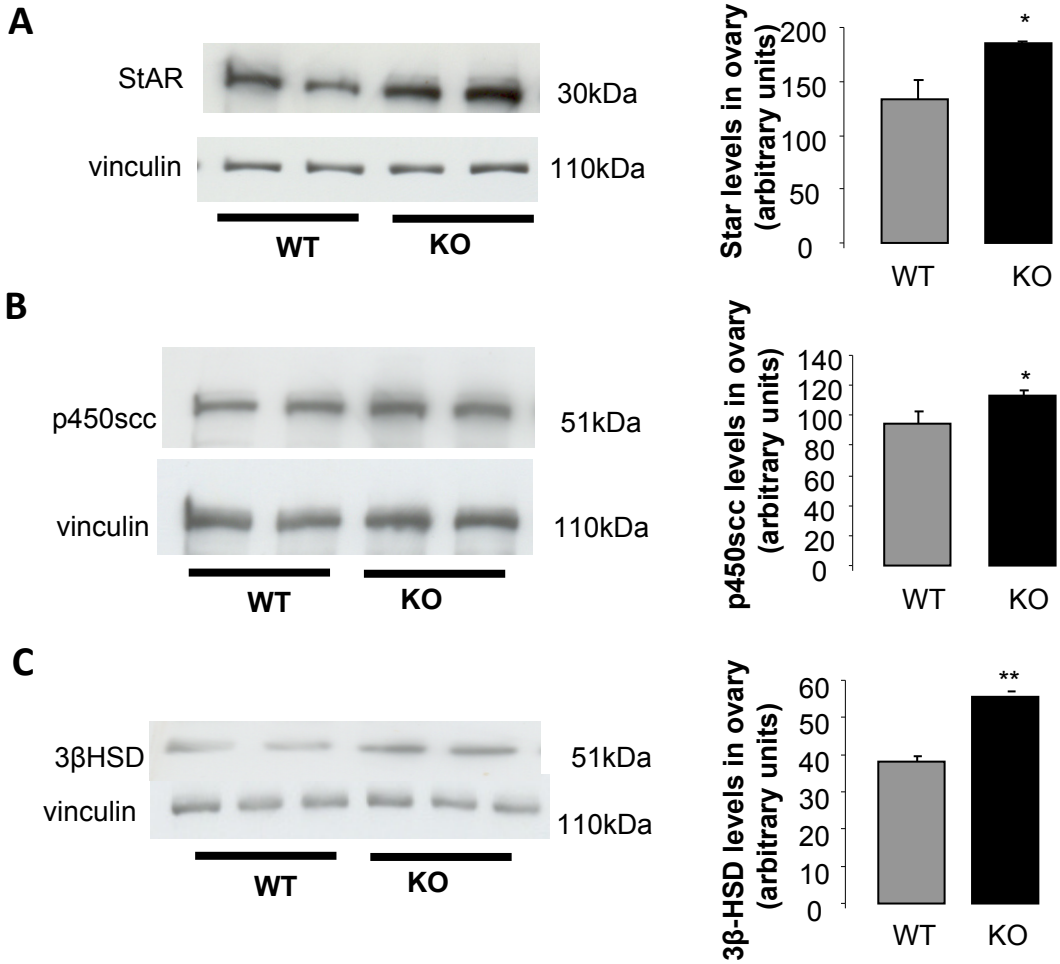
A
StAR
30kDa
vinculin
110kDa
WT
KO
Star levels in ovary (arbitrary units)
200
150
100
50
0
*
WT
KO
B
p450scc
51kDa
vinculin
110kDa
WT
KO
p450scc levels in ovary (arbitrary units)
140
120
100
80
60
40
20
0
*
WT
KO
C
3βHSD
51kDa
vinculin
110kDa
WT
KO
3β-HSD levels in ovary (arbitrary units)
60
50
40
30
20
10
0
**
WT
KO

Figure 10

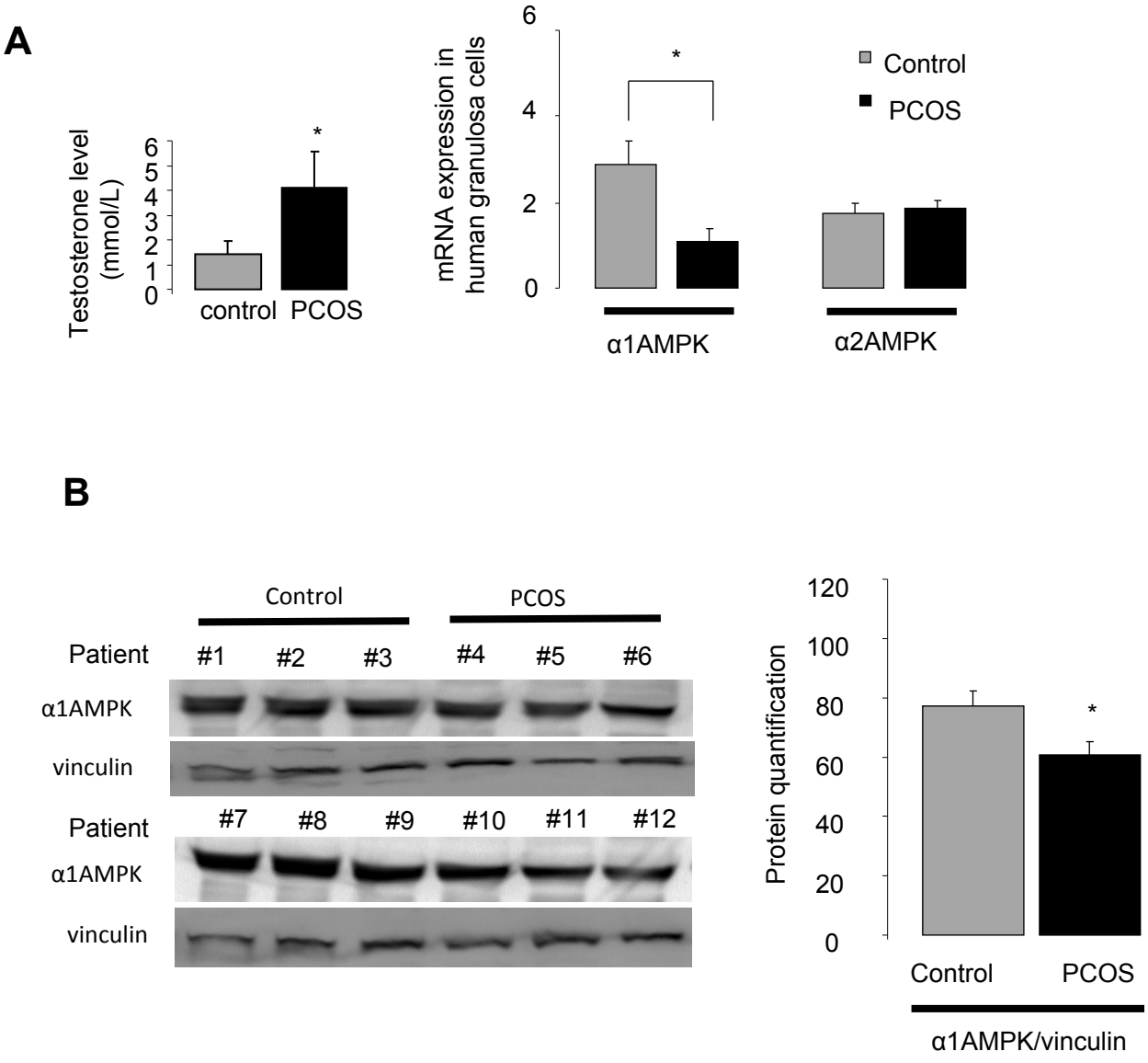
A
Testosterone level (mmol/L)
6
5
4
3
2
1
0
*
control
PCOS
mRNA expression in human granulosa cells
6
4
2
0
*
Control
PCOS
α1AMPK
α2AMPK
B
Control
PCOS
Patient
#1
#2
#3
#4
#5
#6
α1AMPK
vinculin
Patient
#7
#8
#9
#10
#11
#12
α1AMPK
vinculin
Protein quantification
120
100
80
60
40
20
0
*
Control
PCOS
α1AMPK/vinculin

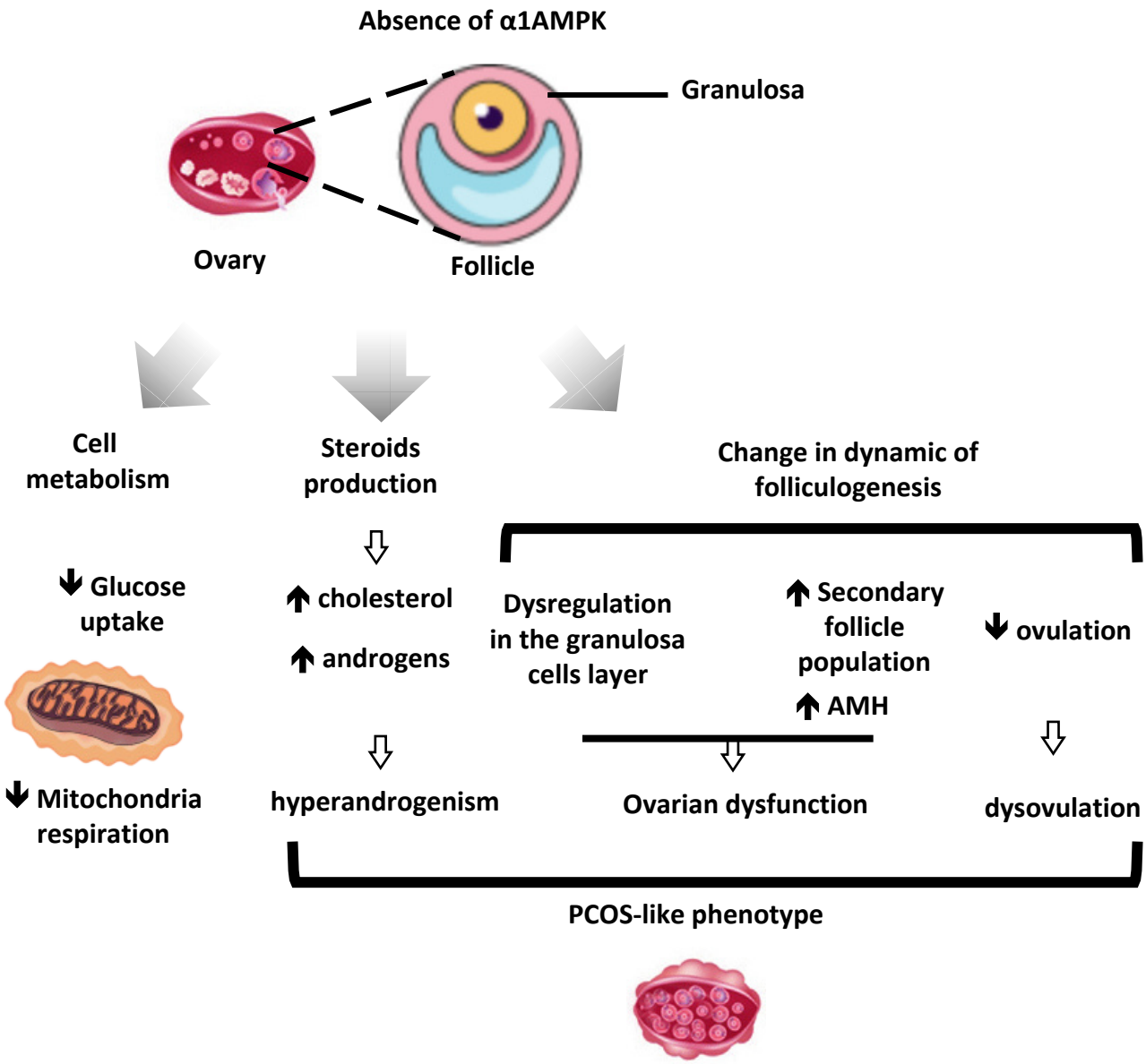
Absence of α1AMPK
Granulosa
Ovary
Follicle
Cell metabolism
Steroids production
Change in dynamic of folliculogenesis
Glucose uptake
cholesterol
androgens
Dysregulation in the granulosa cells layer
Secondary follicle population
AMH
ovulation
Mitochondria respiration
hyperandrogenism
Ovarian dysfunction
dysovulation
PCOS-like phenotype

Suppl Figure 1

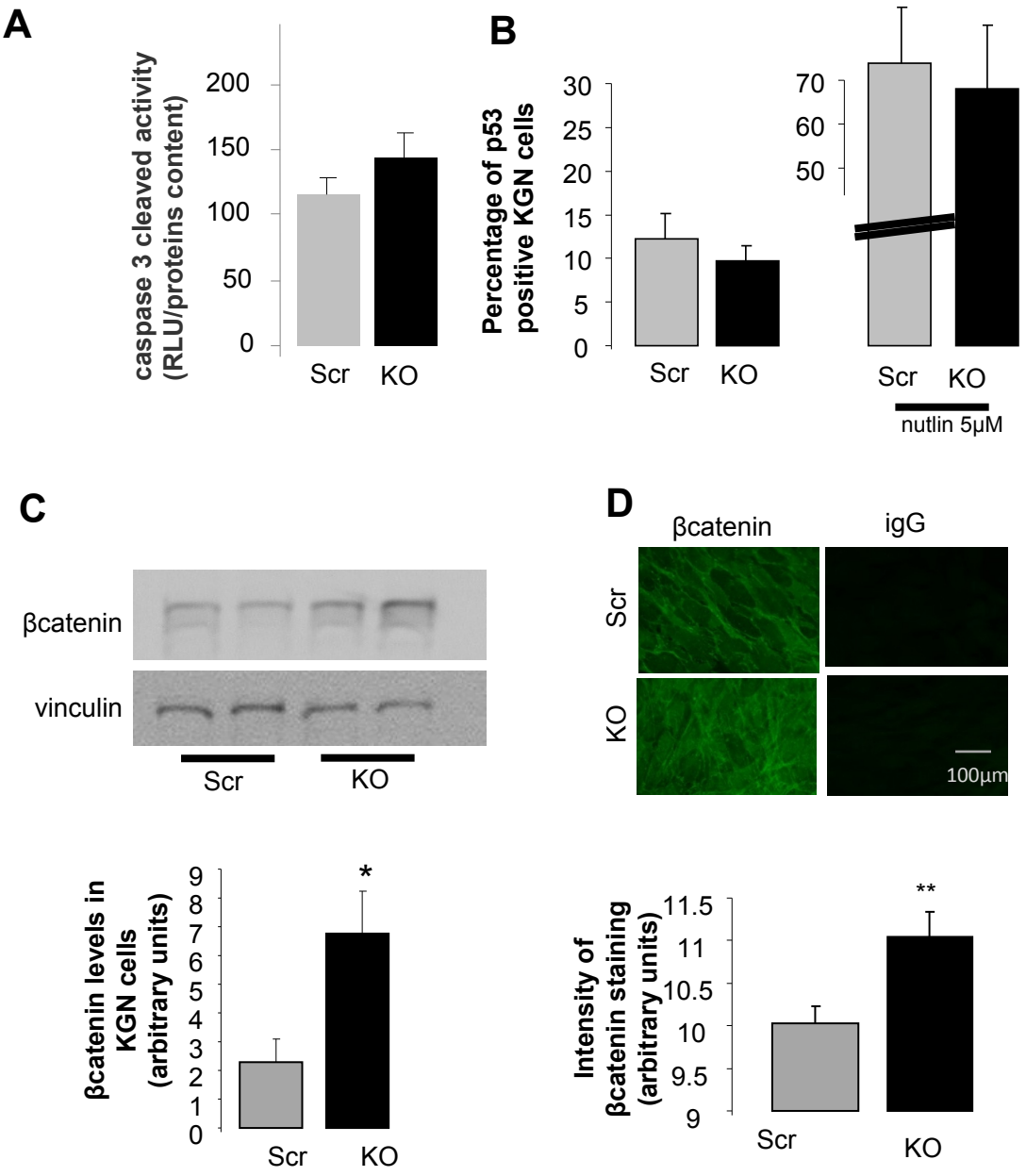

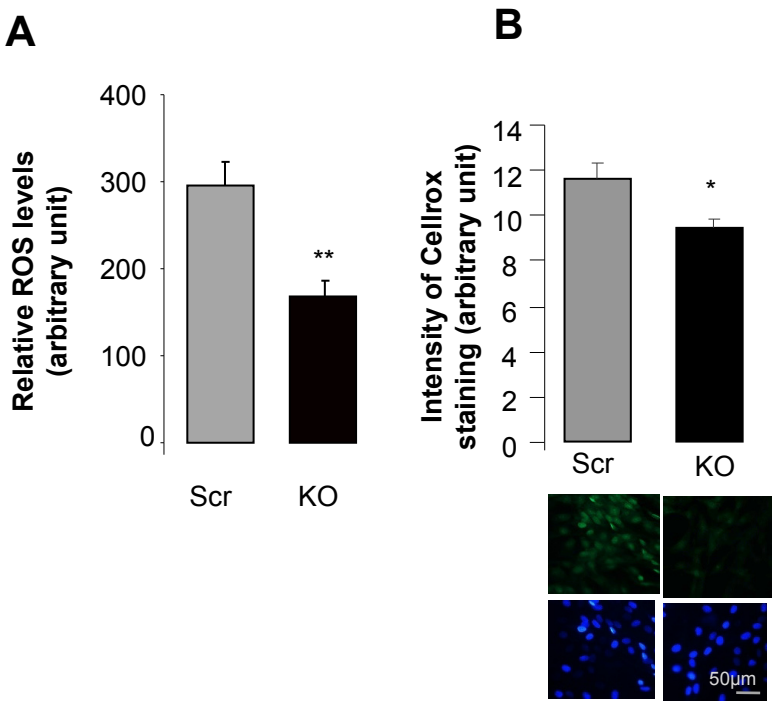
A
Relative ROS levels (arbitrary unit)
400
300
200
100
0
**
Scr
KO
B
Intensity of Cellrox staining (arbitrary unit)
14
12
10
8
6
4
2
0
*
Scr
KO
50μm

Suppl Figure 3

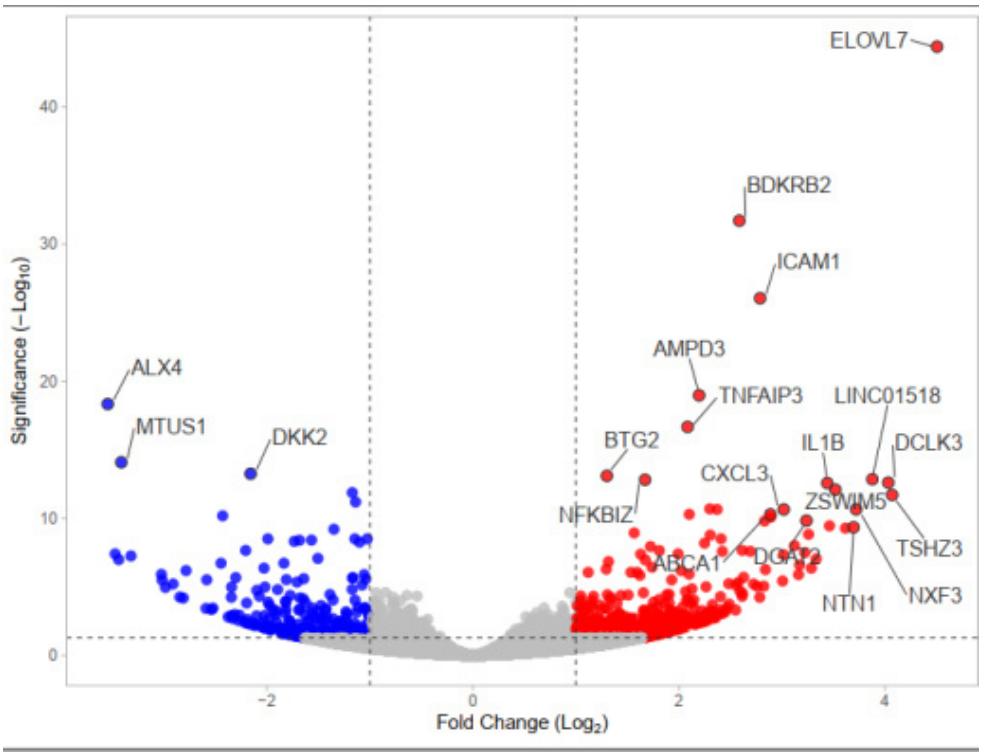

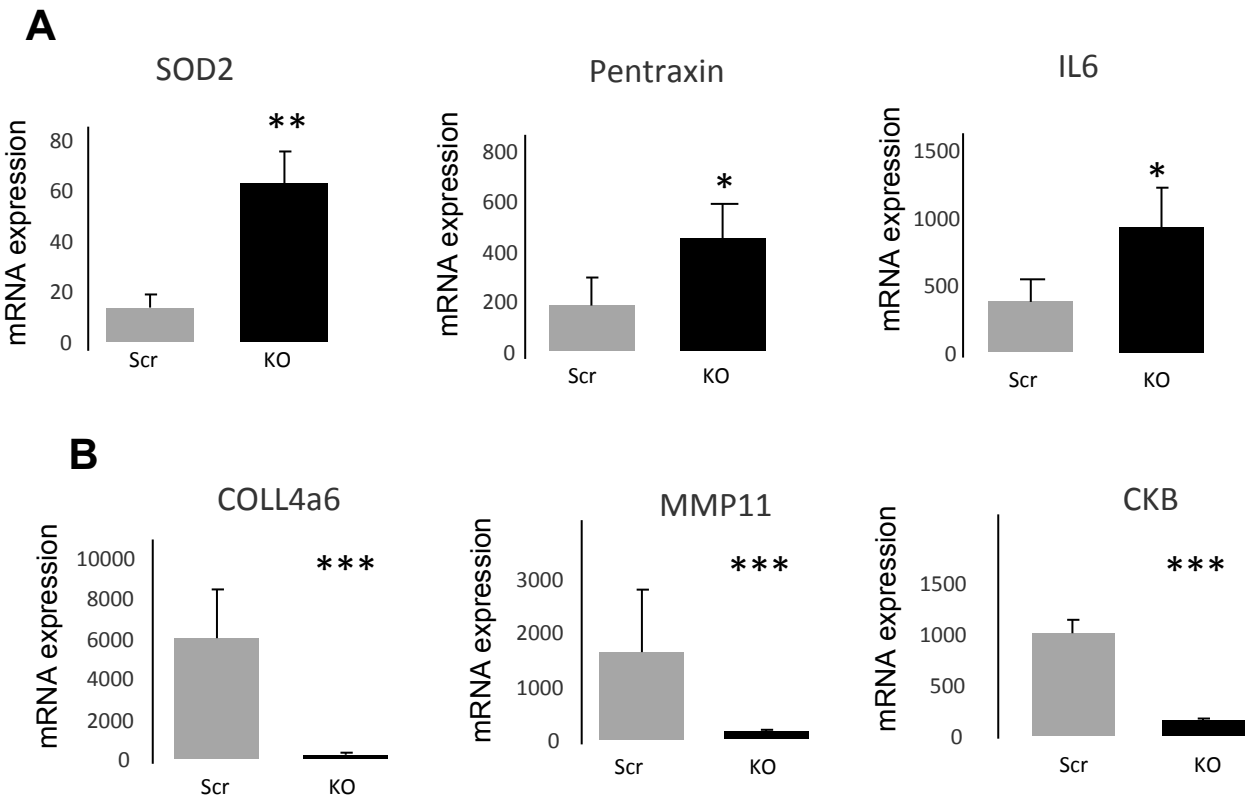
A
SOD2
mRNA expression
80
60
40
20
0
**
Scr
KO
Pentraxin
mRNA expression
800
600
400
200
0
*
Scr
KO
IL6
mRNA expression
1500
1000
500
0
*
Scr
KO
B
COLL4a6
mRNA expression
10000
8000
6000
4000
2000
0
***
Scr
KO
MMP11
mRNA expression
3000
2000
1000
0
***
Scr
KO
CKB
mRNA expression
1500
1000
500
0
***
Scr
KO

Suppl Figure 6

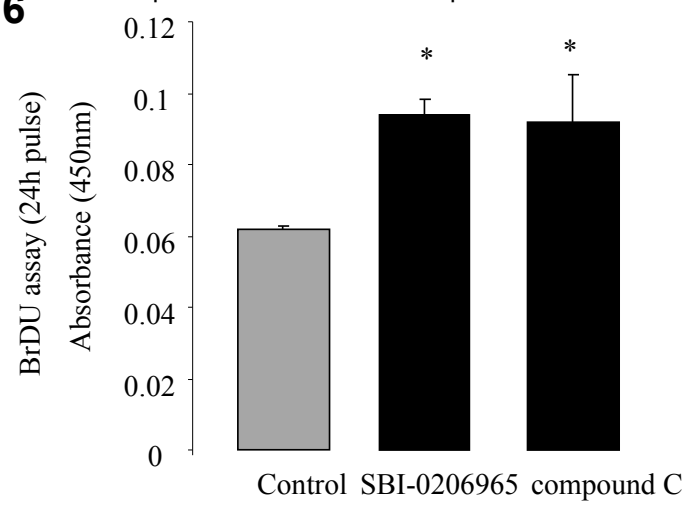

Suppl Figure 7

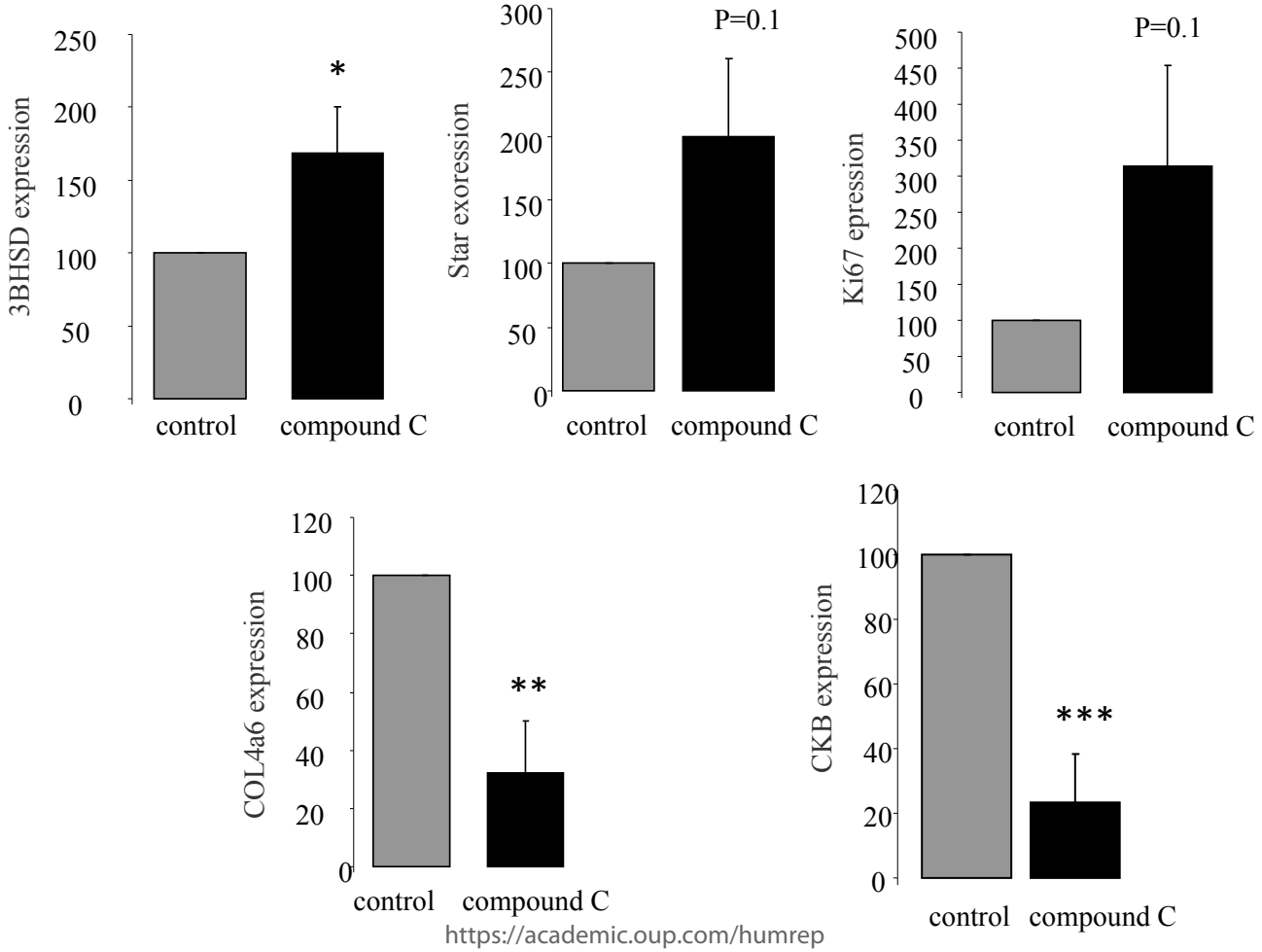

Suppl Figure 8

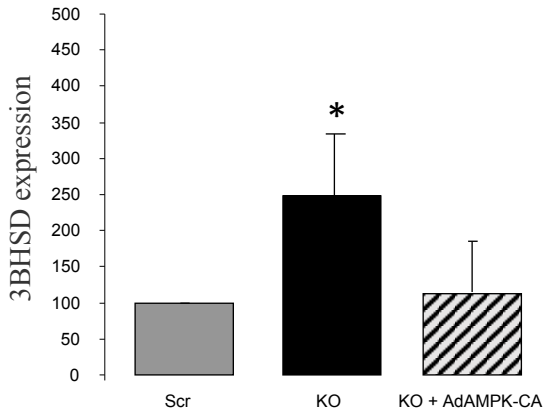

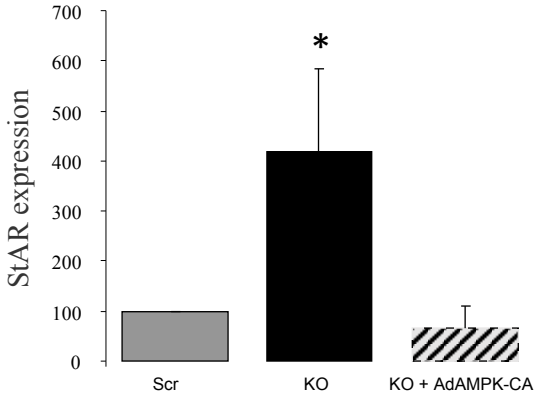

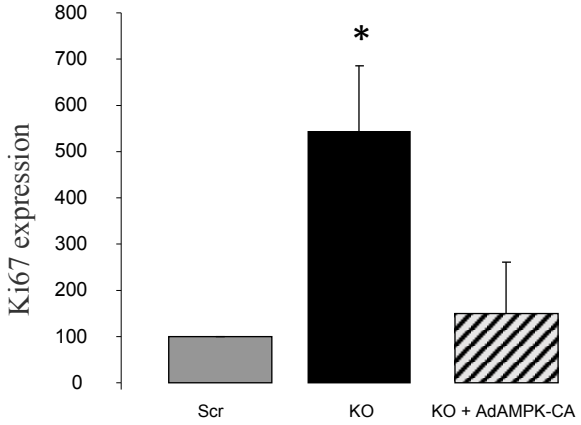

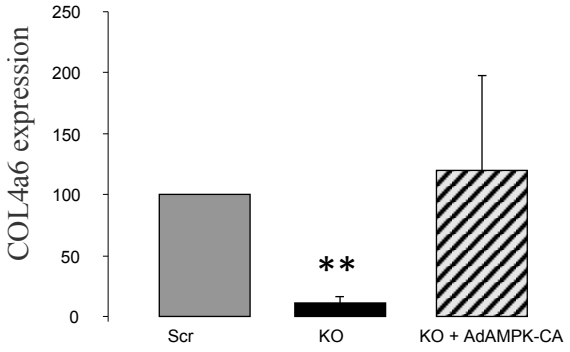

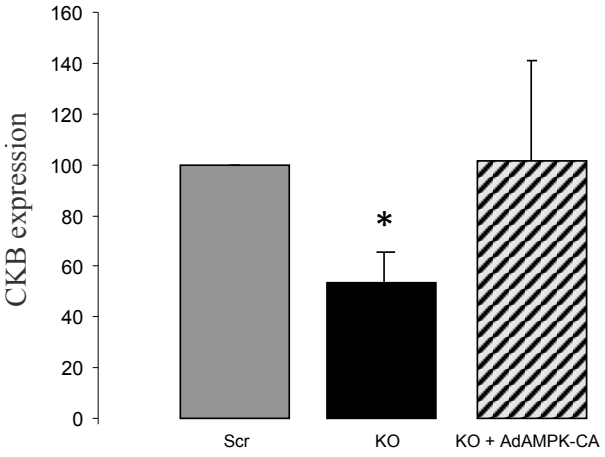

Suppl Figure 9